7-24-2012

# P-N Junction Oxide Nanoparticle as a Novel Photocatalyst for Solar Applications

Bedanga B T Sapkota

# P-N JUNCTION OXIDE NANOPARTICLE AS A NOVEL PHOTOCATALYST FOR SOLAR APPLICATIONS

by

Bedanga BT Sapkota

A Thesis

Submitted in partial fulfillment of the

Requirements for the Degree of

Master of Science

Major: Physics

The University of Memphis

August 2012

## ABSTRACT

Sapkota, Bedanga B T. MS. The University of Memphis. August 2012. p-n junction oxide nanoparticle as a novel photocatalyst for solar applications. Major Professor: Sanjay R. Mishra.

Due to the spectral limitation of popular photocatalysts (PC) $TiO_2$ and ZnO, there is quest for modification of the existing PC to enhance their photocatalytic performance. It has been demonstrated that the coupled nanostructured semiconductors in the form of nanocomposites (NC) enhance the performance by the mutual charge transfer of carriers between each semiconductor components with compatible chemical and electrical properties. ZnO (Bg: 3.37 eV) n-type semiconductor, is most important PC because of its high photosensitivity and stability. CuO (Bg: 1.85 eV), a p-type semiconductor, can be used in conjunction with ZnO to further improve its photocatalytic activity (PCA). Herein, a p-n junction oxide photocatalyst was synthesized by using a simple ball milling technique. The structural, optical, and surface properties of the p-n junction photocatalyst CuO/ZnO were characterized by X-ray powder diffraction (XRD), transmission electron microscopy (TEM), UV-Vis spectroscopy, Zetasizer Nano ZS (Malvern). The PCA of the photocatalyst was evaluated by photocatalytic oxidation of Methylene Blue (MB).

Our study demonstrates a novel p-n junction oxide photocatalyst CuO (wt.10%)/ZnO having superior PCA for the degradation of model dye under the illumination of UV-Vis light. The MB solution was degraded by 100% within 15 min by the use of CuO (wt. 10%)/ZnO photocatalyst. The enhanced PCA is anticipated from many micros p-n junction formed between ZnO-CuO upon ball milling, which helps in efficient electron/hole pair charge separation upon excitation.

## ACKNOWLEDGEMENTS

For the past two years there have been several people who have been there for me. Without their support and help this work would not have been completed. I would first and foremost like to thank my supervisor, Dr. Sanjay R Mishra for his guidance, suggestions, support, motivation and continuous encouragement throughout this work. I sincerely appreciate all of his efforts. I am extremely grateful to Dr. M. Shah Jahan and Dr. Lam Yu for their cooperation and suggestions. Thanks also must go to all the staffs of Department of Physics, University of Memphis for their constant support. I appreciate my colleagues Binod Rai, Armstrong Wilson, Jibanath Dahal, Ganesh Pokhrel, and Lijia Wang for their cooperation and help. I would also like to thank my housemate Sudhir Upreti.

At last but certainly not the least, I would like to thank my parents, wife and brothers for their constant inspiration and moral support. I would like to dedicate this thesis to my parents. You truly are wonderful parents and I will forever be grateful for everything you have done for me throughout my life.

## TABLE OF CONTENTS

## ABBREVIATIONS USED

| | | |
|---|---|---|
| AOP | : | Advanced oxidation process |
| BM | : | Ball milling |
| BMT | : | Ball milling time |
| CB | : | Conduction band |
| CWA | : | Chemical warfare agent |
| $e^-$ | : | electron |
| eV | : | electron volt |
| g | : | gram |
| $h^+$ | : | hole |
| MB | : | Methylene blue |
| min | : | minute |
| mL | : | milliliter |
| MO | : | Methyl orange |
| NC | : | nanocomposite |
| nm | : | nanometer |
| $NO_x$ | : | Nitrogen oxides (NO and $NO_2$) |
| PC | : | Photocatalyst |
| PCA | : | Photocatalytic activity |
| PCD | : | Photocatalytic degradation |
| PCE | : | Photocatalytic efficiency |
| PD | : | Photodegradation |
| PDE | : | Photodegradation efficiency |

| | | |
|---|---|---|
| PL | : | Photoluminescence |
| ps | : | picosecond |
| RB | : | Rhodamine B |
| RB-19 | : | Reactive Blue 19 |
| TEM | : | Transmission electron microscopy |
| UV | : | Ultraviolet light |
| VB | : | Valence band |
| VOC | : | Volatile organic compound |
| XRD | : | X-ray diffraction |
| ZP | : | Zeta potential |

## LIST OF FIGURES

The scientific man does not aim at an immediate result. He does not expect that his advanced ideas will be readily taken up. His work is like that of the planter—for the future. His duty is to lay the foundation for those who are to come, and point the way.
— Nikola Tesla

# CHAPTER 1

# INTRODUCTION

## 1.1) Nanoparticle and Its Importance as Photocatalyst

"Small is beautiful", today we know that small is not only beautiful but also powerful. Nanoparticles are particles that have at least one dimension in less than 100 nm range. Because of their small size, nanoparticles exhibit the novel properties. As the particle size decreases, surface to volume ratio increases. Mathematically, for spherical particle, volume (V) is given by

$V=\frac{4}{3}\pi R^3$, where R is the radius of the spherical particle.

The total surface area (S) is given by

$S=4\pi R^2$

Now, surface to volume ratio,

$$\frac{S}{V}=\frac{3}{R}$$

This shows that as the radius of the spherical particle decreases, surface to volume ratio increases. Nanometer–sized particles have very different physical and chemical properties from bulk materials. As catalysis, their Catalytic activity is enhanced not only because of their surface area but also change of surface properties such as surface defects. When the crystallite dimension of semiconductor particle falls below critical radius ~ 50 nm, the charge carriers behave quantum mechanically like simple particles in a box.

This confinement produces a quantization of discrete electronic states and increases the effective band gap of the semiconductor. Additionally, for the degradation of pollutant by a catalyst it requires that pollutant to be adsorbed or very close to the surface of the material. This means greater the surface area of the material, the more pollutant it can adsorb. Thus, the nanoparticulate materials are promising candidate as they vastly increase the surface area.

## 1.2) Photocatalysis

Photocatalysis is a light-induced catalytic process whereby photogenerated electron-hole pairs in a semiconductor undergo redox reactions with molecules adsorbed onto the surface, thereby breaking them into smaller fragments. In simple words; photocatalysis is a simultaneous oxidation and reduction process. Figure 1.1 shows an illustration of photocatalysis process in the presence of UV light. Absorbed pollutant on the surface of the photocatalys breaks down during this process and hence the removal of pollutant from waste water. Photcatalysis reactions may occur homogeneously or heterogeneously, but heterogeneous photocatalysis is far more intensively studied in recent years because of its potential use in a variety of environmental and energy related applications as well as in organic synthesis [1]. In heterogeneous photocatalysis, the reaction scheme implies the formation of an interface between a solid photocatalyst (metal or semiconductor) and a fluid containing the reactant and products of the reaction. Therefore, the term “heterogeneous photocatalyst” is mainly used in cases where a light absorbing semiconductor photocatalyst is utilized, which in contact with either liquid or a gas phase.

The heterogeneous photocatalysis, one of the Advanced Oxidation Processes (AOP), permits the total degradation (mineralization) of the most toxic organic molecules in aqueous solution in the presence of a catalyst. These processes are based on the generation of hydroxyl radicals ($HO^{\bullet}$) which are the principal agents responsible for the oxidation of numerous aqueous organic Contaminants [2]. Photocatalyis with metal oxide-semiconductor nanostructure has been an area of research interest over the last couple decades with titania receiving the most attention [3-6]. The advantage of this oxide semiconductor photocatalyst is that they lead to the total mineralization of organic contaminants.

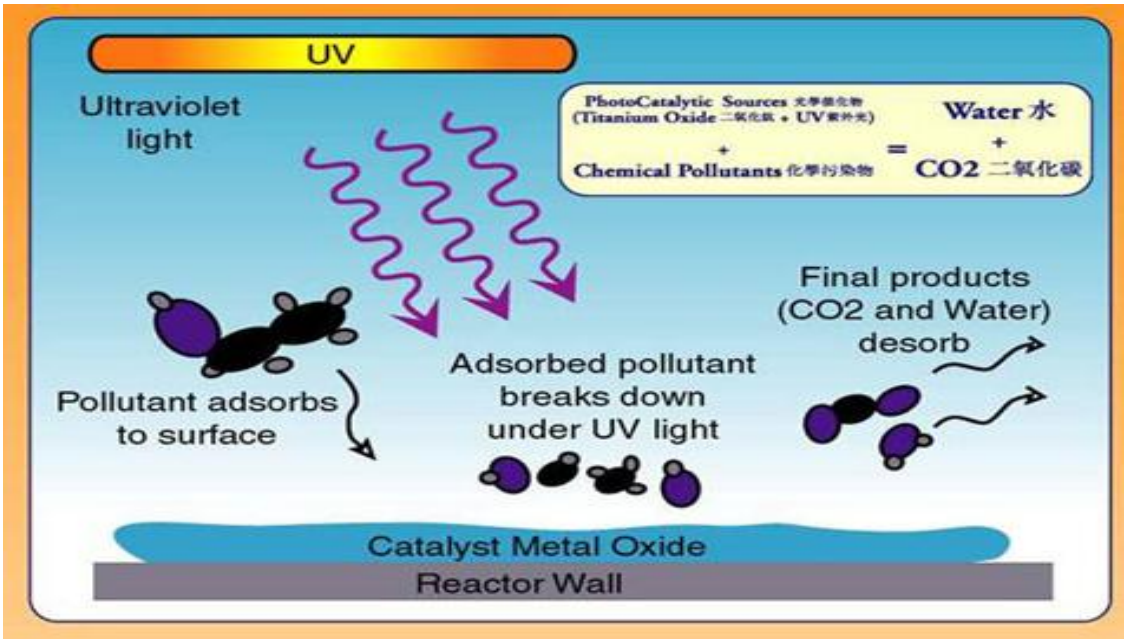


**Figure1.1**: Break down of the adsorbed pollutant during photocatalysis process in the presence of UV light.

### 1.3) Photocatalyst

The redox couple capable of promoting both the oxidation and reduction reactions can act as photocatalyst. Semiconductors are predominantly useful as photocatalyst because of a favorable combination of electronic structure, light absorption properties, charge transport characteristics and excited-state lifetimes [1].

In semiconductor photocatalyst, excitation of electron from the valence band to the conduction band is accomplished by the absorption of photon energy equal to or greater than the band gap energy of the semiconductor. Light-induced generation of electron-hole pairs is a prerequisite step in all semiconductor-mediated photocatalysis process. Transfer of an electron to or from a substrate absorbed onto the light-activated semiconductor is probably the most crucial step in photocatalysis process, and its efficiency determines to a large extend the ability of the semiconductor to serve as a photocatalyst for a given redox reaction [1]. Additionally, the efficiency of the electron transfer reaction is a function of the position of the semiconductor's conduction and valence band-edges relative to the redox potentials of the absorbed substrates. Thus, widely used semiconductor photocatalysts are those which have a suitable band gap in UV and visible regions. Some examples are shown in Fig 1.2.

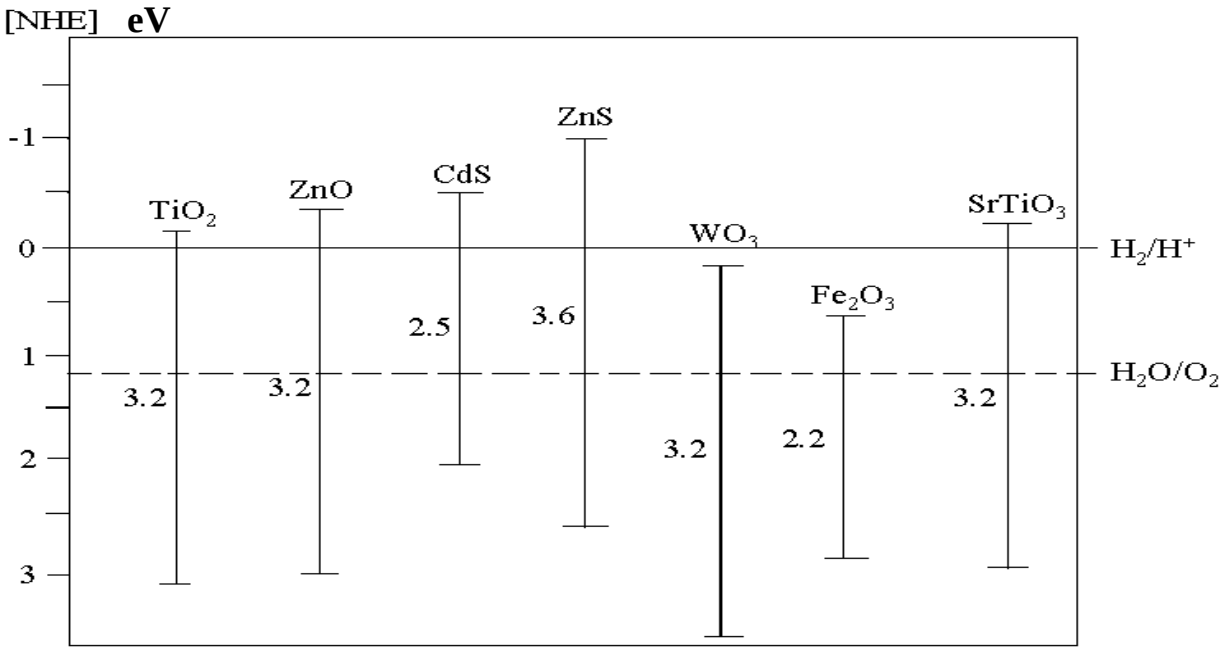


**Figure 1.2**: Positions of bands of semiconductors relative to the standard potentials of several redox couples.

From the above figure, zinc oxide which has a band gap of 3.2 eV falls in the UV-region whereas iron oxide, band gap 2.2 eV, falls in the visible region. The ideal photocatalyst should possess the following properties such as:

(I) Photoactivity

(II) biological and chemical inertness

(III) stability toward photocorrosion

(IV) suitability towards visible or near UV light

(V) low cost

(VI) Lack of toxicity [7].

Figure 1.3 shows the schematic of photocatalytic mechanism of widely used photocatalyst $TiO_2$. In photocatalysis, light of energy greater than the band gap of the

semiconductor, excites an electron from the valence band to the conduction band (Fig 1.3). The band gap of TiO2 (anatase) is 3.2 eV, therefore UV light (< 380 nm) is required to initiate the photocatalytic process. Light (< 380 nm) excites an electron ($e^-_{CB}$) to the conduction band generating a positive hole ($h^+_{VB}$) in the valence band. Alternatively the charge carriers can migrate to the catalyst surface and initiate redox reactions on the adsorbates.

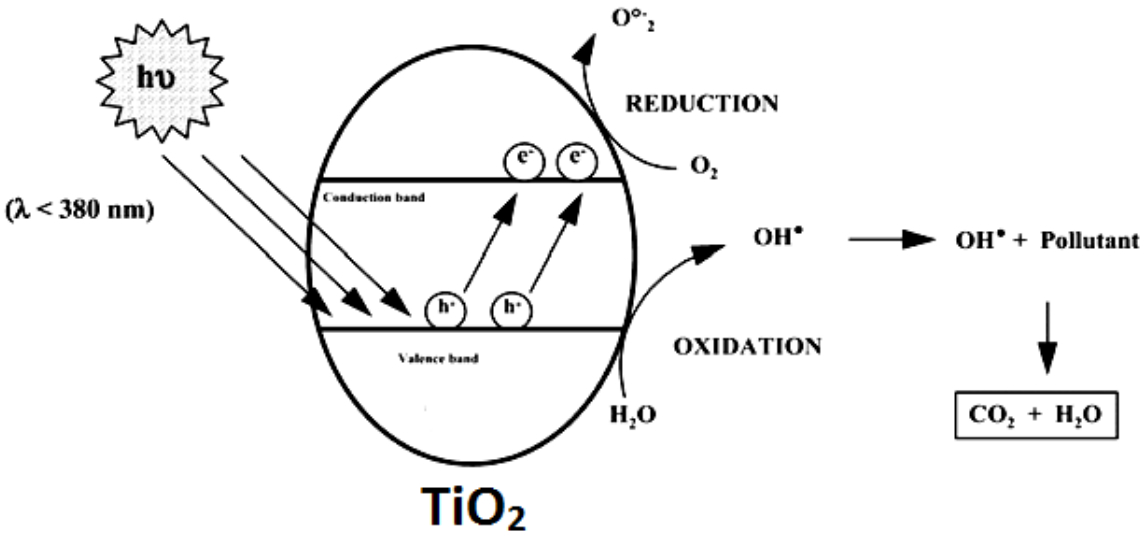


**Figure 1.3**: A schematic diagram showing photocatalytic process of widely used photocatalyst Titania.

## 1.4) Applications of Photocatalysts

Photocatalysts have several potential applications in wide range of areas. Schematic representation of applications of photocatalyst is given below in Fig 1.4. The number of new applications of photocatalyst based on its photoelectrochemical properties towards environmental usage is increasing. Some of the most important applications are as follows:

### 1.4.1) Photocatalysis for water treatment

Widespread water source contamination is a major problem associated with environment. Problematic substances in wastewater can include organic matter and/or different trace contaminants. Trace metal such as mercury (Hg), chromium (Cr), lead (Pb) and others metals are considered to be highly health hazardous. Thus, removing these toxic metals is essentially important for human health and water quality. The environmental applications of heterogeneous photocatalysis include removing heavy metals such as mercury (Hg), chromium (Cr), lead (Pb), cadmium (Cd), lead (Pb), Arsenic (As), nickel (Ni) and cupper (Cu) [8]. In drinking water production the contamination with microbes is the major problem that needs to be addressed. Solar energy is a clean and renewable resource and is ideal for environmental and sustainable applications. Solar photocatalysis had been identified as the main technology breakthrough for water treatment and purification. Photocatalytic systems in AOPs may complement existing techniques in the removal of trace contaminants.

### 1.4.2) Destruction of Warfare Agents

Photocatalysts have the potential to decompose various hazardous substances at least in mild conditions. Researchers have examined the photocatalytic degradation of chemical warfare agents (CWAs) [9]. Results indicate that photocatalysts may support the detoxification of hazardous compounds.

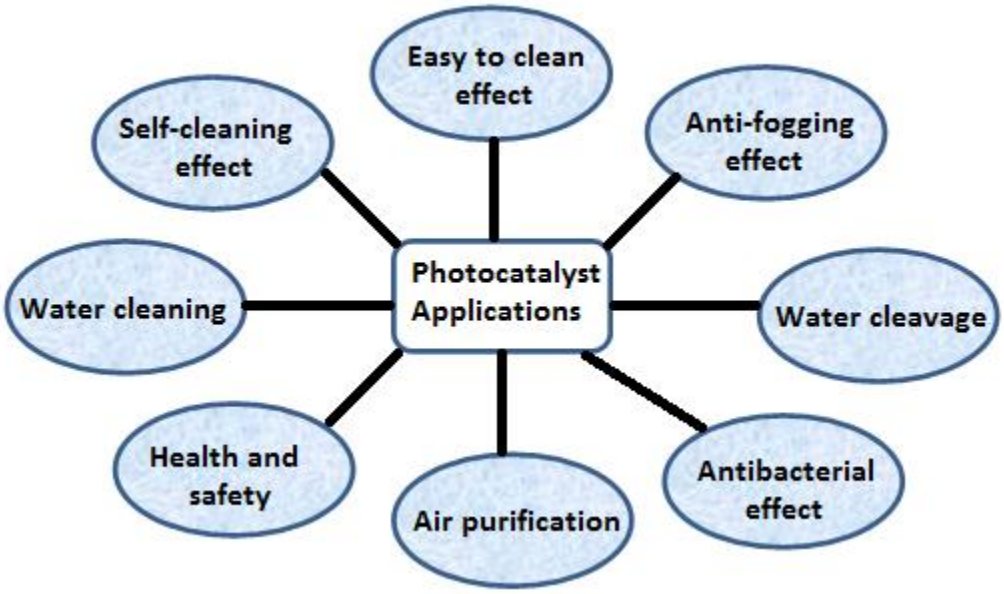


**Figure 1.4**: Representing basic applications of photocatalyst

### 1.4.3) Self-cleaning agents

Photocatalysis has a great potential to cope with the increasing pollution by traffic. Self-cleaning surfaces, air purification and sterilization are the three major applications of

photocatalysis besides waste water treatment. Meanwhile photocatalytic cement and glass are well established.

"TX Active®" of the Italcementi Group is photocatalytic cement, able to reduce organic and inorganic pollutions in the air or on surfaces. It is particularly efficient in the decomposition of nitrogen oxides ($NO_X$) based substances from industry, transport and residential heating systems [9]. Application examples exist in US, Italy, France, Belgium, and the Morocco. The widely used photocatalyst for such applications is $TiO_2$. It is well known that oxides of Nitrogen are the most important pollutants produced by traffic and play a major role in the formation of smog and ozone. The following chemical reactions show the oxidation of NO and $NO_2$ in the presence of sunlight and $TiO_2$ photocatalyst.

$$NO + OH^{\bullet} \xrightarrow{h\nu, TiO_2} NO_2 + H^+$$

$$NO_2 + OH^{\bullet} \xrightarrow{h\nu, TiO_2} NO_3^- + H^+$$

Parameters that influence the oxidation reaction are the relative humidity and the temperature. At higher temperatures, the conversion will be better [10]. The relative humidity is important, since the water in the atmosphere plays a role in the adhesion of the pollutants at the surface and therefore also the conversion rate. In the case of a higher relative humidity, the conversion will be lower. Optimal conditions are therefore reached on hot summer days with high temperatures and low relative humidity. It is also on those days that the risk on smog during the summer is the highest and thus the efficiency of the air purification is the highest [10].

"Pilkington Activ$^{TM}$" is a self-cleaning glass by Pilkington Ltd. A photocatalytic coating on the outside surface cleaves organic pollutants upon UV-illumination; dirt is

thus easily washed off by rain [11]. Pilkington Activ™, a Self-cleaning glass, by Pilkington Ltd is as shown in Fig 1.5. The difference between the normal and Pilkington Activ™ glass after rainfall has shown in the Fig. In practice, a thin film of nanoparticulate photocatalyst (mainly titanium dioxide) is coated onto panes of glass (it is so thin that it is transparent). The glass is in the normal course of events, acquiring dirt. The titanium dioxide on the glass, once exposed to sunlight, produces hydroxyl radicals which degrade any surface-adsorbed dirt. Once washed down with rain, this decomposed dirt is removed and the glass is ready for another cycle.


**Figure 1.5**: Self-cleaning windows from Pilkington Activ™.

(Source: http://www.pilkingtonselfcleaningglass.co.uk/trade/; 22-May-2012)

### 1.4.4) Air purification

A variety of air pollutants are known or suspected to have harmful effects on human health and environment. The principal pollutants emitted by vehicles are carbon monoxide, oxides of nitrogen (NOx), volatile organic compounds (VOC's) and particulates. These pollutants have an increasing impact on the urban air quality. Photocatalytic surfaces have the potential application to act against such variety of air pollutants and odours, VOC, formaldehyde, ammonia and inorganic gaseous substances such as nitrogen- or sulphur-oxides ($NO_X$, $SO_X$) [9]. Meanwhile a variety of technical products are commercially available. Applications include photocatalytic components for air filters, ventilation, and air conditioning systems via active decomposition of cigarette smoke or automotive and industrial exhaust to general air purifying effects of larger photoactive building elements.

### 1.4.5) Environment, Health, and Safety aspects

Titania photocatalyst in its bulk form is successfully used as an additive in widely distributed consumer products such as cosmetics, sun screens, toothpastes etc. [9]. A review of literature on nano $TiO_2$ has illustrated that, in relation to inhalation, this material demonstrates increased toxicity as particle size decreases due to the increasing surface area. However, the ability of particles to exert toxicity within the body depends on the level of exposure, and the subsequent behavior after it enters the body. Dermal exposure studies to date have not yet demonstrated any penetration or toxicity via this route [9].

### 1.5) Need of Semiconductor Photocatalyst

In recent years, quality of drinking water has become a major concern worldwide due to increase in population and decreasing energy resources. Due to this reason, the efficient treatment of wastewater has become immediate important among the science communities around the globe. Conventional treatment of biological wastewater is not effective. Additional process like coagulation, membranes, or adsorption have been applied which results in complications like production of toxic, membranes fouling, high cost. Ideally, an effective wastewater treatment is to mineralize completely all the toxic contaminants in wastewater without leaving any hazardous residues. In addition, the wastewater treatment process should be cost-effective and feasible for large scale applications [12, 13].

Unfortunately, by the time being, only a limited number of employed treatment technologies such as activated carbon and biological methods, which somewhat fulfilled the requirements [12]. Thus, it is necessary to find an alternative solution which may offer a prominent route in industrial wastewater treatment process. Semiconductor photocatalysis has become more and more attractive and important since it has a great potential to contribute to such environmental problems [14]. Advantages of semiconductor photocatalyst are as follows:

I) high surface area

II) morphology

III) presence of surface states

IV) wide band gap

V) position of the VB and CB edges

One of the most important aspects of environmental photocatalysis is the selection of semiconductor materials like ZnO and $TiO_2$, which are close to being two of the ideal photocatalyst in several aspects. For example, they are relatively inexpensive, and they provide photo-generated holes with high oxidizing power due to their wide band gap energy. As a well know photocatalyst, ZnO has received much attention in the degradation and complete mineralization of environmental pollutants [15, 16, 17,18]. Since ZnO has almost the same band gap energy (3.2 eV) as $TiO_2$, its photocatalytic capacity is anticipated to be similar to that of $TiO_2$. However, in the case of ZnO, photocorrosion frequently occurs with the illumination of UV light, and this phenomenon is considered as one of the main reasons for the decrease of ZnO photocatalytic activity in aqueous solutions [19, 20]. However, some studies have confirmed that ZnO exhibits a better efficiency than $TiO_2$ in photocatalytic degradation of some dyes, even in aqueous solution [21,22]. There is problem with these photocatalyst, problem associated with titania is the recombination time of photogenerated electrons and holes. The electron-hole recombination time is on the order of $< 30$ ps due to which photodegradation efficiency cannot exceed in significant amount. Recombinations are of two types- volume recombination and surface recombination. Former can be reduced by preparing oxides in nanoscale whereas latter one can be avoided by doping some foreign material like metal, non-metals and by coupling oxides with other semiconductors etc.

Figure 1.6 shows the photoexcitation process followed by deexcitation events in a semiconductor photocatalyst. The pathways marked as (a) and (b) illustrate the unwanted recombination of the charges both in the volume (a) and on the surface (b). On the other hand, (c) and (d) pathways are the desirable deexcitation through the redox reaction of

the electrons and holes. It was also noted that photocatalytic activity of modified ZnO sample was five times higher than the unmodified sample [23].

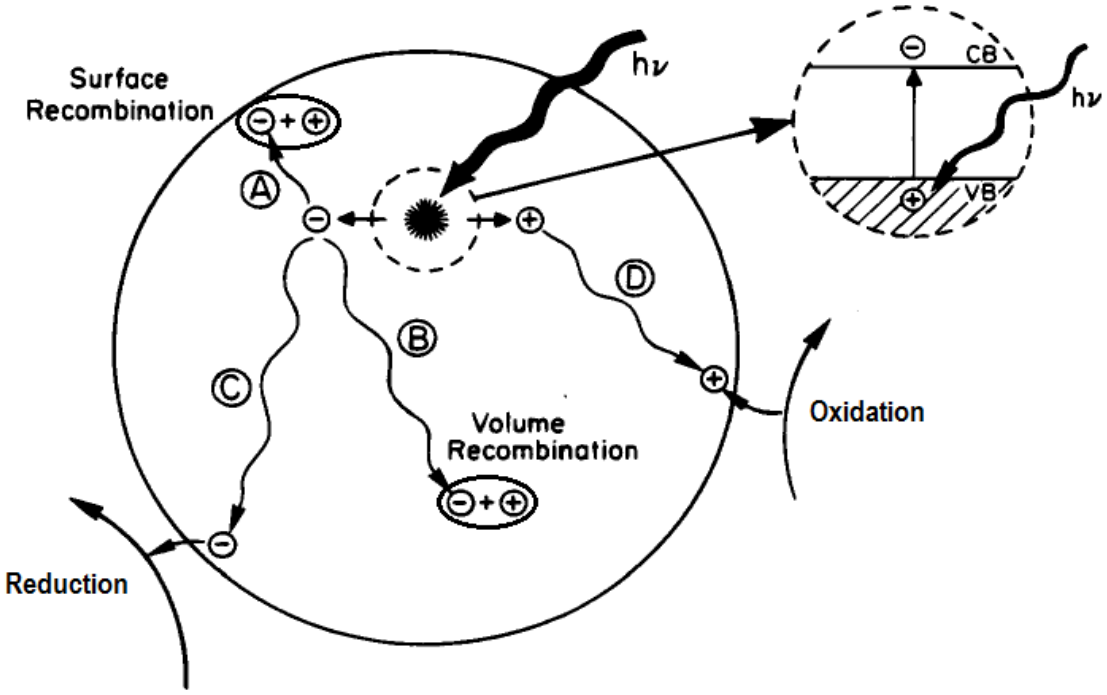


**Figure 1.6**: Schematic photoexcitation in a semiconductor photocatalyst followed by the deexcitation pathways.

## 1.6) Surface Modifications of Semiconductor Photocatalyst

Some strategies which are in vogue to enhance photocatalytic activity of the photocatalyst are as follows:

### 1.6.1) Metal semiconductor modification

The modification of semiconductors with noble metals has attracted significant attention especially in heterogeneous photocatalysis. Metallic promoter enhances the photocatalytic reaction by trapping the electron from the conduction band of the semiconductor photocatalyst and slows recombination reaction. Figure 1.7 shows the schematic diagram of metal semiconductor modification. Once the noble metal particles contact with semiconductor surface, the Fermi level of noble metal shifts to the semiconductor Fermi level.

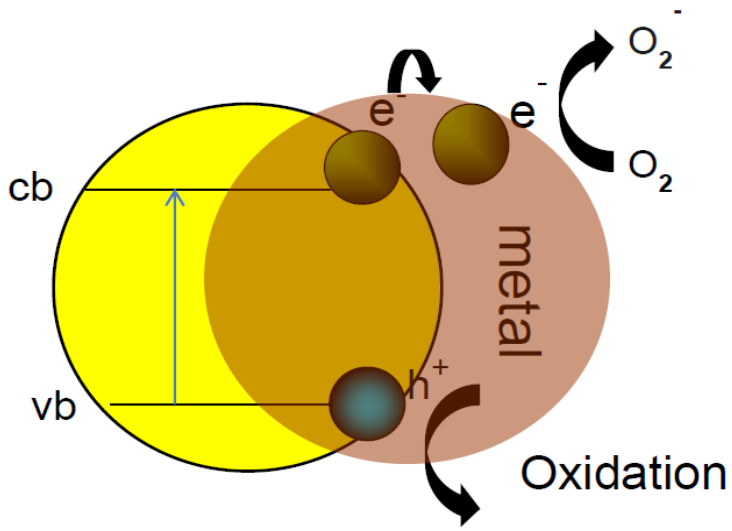


**Figure 1.7**: Schematic diagram showing incorporation of metal with semiconductor photocatalyst for the enhancement of photocatalytic reaction.

After excitation, the electron migrates to the metal where it becomes trapped and electron-hole recombination is suppressed. The hole is then free to diffuse to the semiconductor surface where oxidation of organic species can occur. The metal is

important also due to its own catalytic activity. The metal actually modifies the photocatalytic properties of the semiconductor by changing the distribution of electrons. When two species come in contact the Fermi levels of the metal and semiconductor align causing electrons to flow to the metal from semiconductor. The decrease in the electron density within the semiconductor leads to an increase in the hydroxyl group acidity [24]. This, in turn affects the photocatalytic process on the semiconductor surface. It is also noted that above the optimum metal content the efficiency of the photocatalytic process decreases [25]. This is because higher than optimum amount of noble metal (Au, Ag, Cu etc.) may cover the titanium dioxide and prevent light absorption. In addition, too much silver may mean that the silver acts as a recombination site itself – essentially it will form a bridge between an electron and a hole. Therefore, care must be taken when studies are conducted on a metal-modified semiconductor to work with the quantity of metal which gives the optimum photocatalytic efficiency.

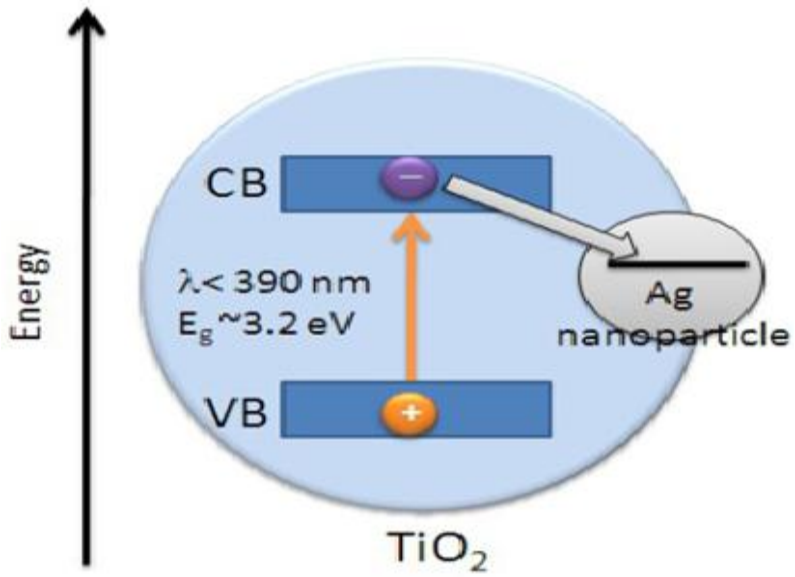


**Figure 1.8**: Mechanism for reduced recombination of $TiO_2$ by modifying its surface using Ag nanoparticle.

(Source: photochemistry portal)

Figure 1.8 shows the schematic diagram of Ag/ $TiO_2$ nanocomposite system. This mechanism could be supported by the report of Sonawane and Dongare [26]. By studying thin films of Au/$TiO_2$ prepared by simple sol-gel dip coating method, they showed that the photocatalytic activity of phenol decomposition could be improved by 2-2.5 times than that of $TiO_2$. Similar experimental results on the photocatalytic activity of Au/$TiO_2$ photocatalyst were reported for the reaction of methylene blue degradation [27].

### 1.6.2) Transition Metal Doping

Dopants influence intrinsic properties of photocatalyst resulting in lowering the band gap and shifting light absorption into visible spectral range. Another benefit of

transition metal doping is the improved trapping of electrons to inhibit electron-hole recombination during illumination. Dopants should be both good electron and hole traps. Only certain transition metals such as $Fe^{3+}$ and $Cu^{2+}$ actually inhibit electron-hole recombination [28, 29]. The concentration of the beneficial transition metal dopants is very small. Other transition metal dopants such as $Cr^{3+}$ create sites which increase electron-hole recombination [30]. It is believed that these transition metals create acceptor and donor centers where direct recombination occurs.

### 1.6.3) Coupled Semiconductor

Another interesting way to increase the efficiency of photocatalytic process is the formation of coupled semiconductor photocatalyst. This system significantly increases the recombination time of photodegenerated electron/hole pairs and extends the energy range of photoexcitation of the system [25]. Improved Sol-gel method and co-precipitation method are used to prepare composite semiconductor photocatalyst such as $TiO_2$-CdS, $TiO_2$-$SnO_2$, $TiO_2$-$WO_3$, $TiO_2$-ZnO, etc.

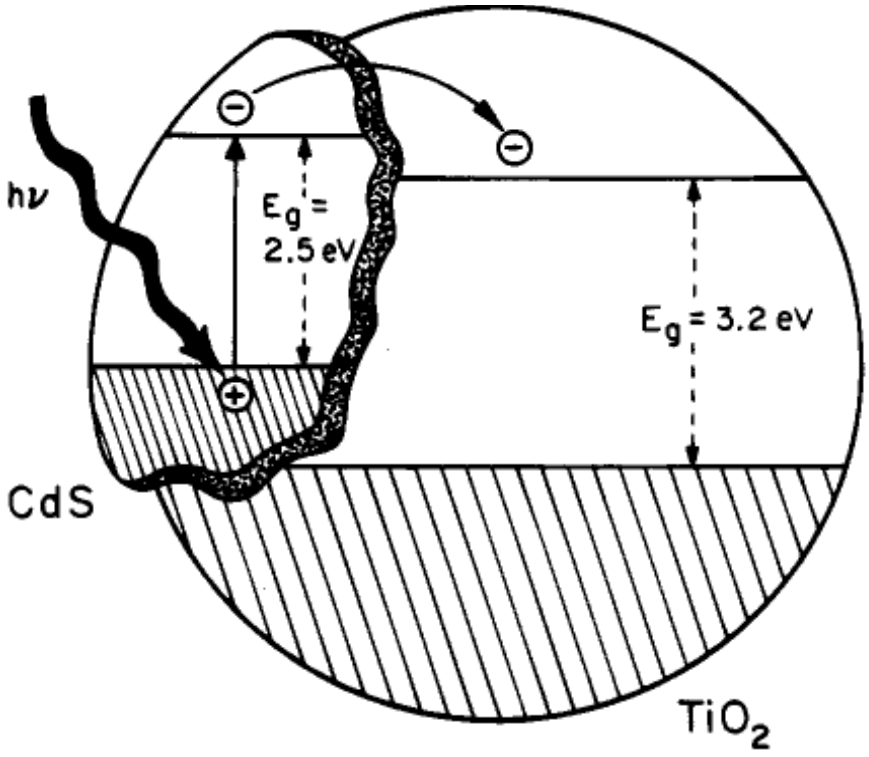


**Figure 1.9**: Schematic illustration of charge transfer in a coupled semiconductor system.

(Source: Surface Science Center)

Figure 1.9 illustrates geometrically and energetically the photoexcitation process for the composite (coupled) semiconductor photocatalyst $TiO_2$-CdS. The energy of the excitation light is too small to directly excite the $TiO_2$ portion of the photocatalyst, but it is large enough to excite the electron from the valence band to conduction band of CdS (Eg = 2.5 eV ). According to the model as shown in the figure, the hole produced in the valence band due to excitation of light remains in CdS particle whereas the electron transfers to the conduction band of $TiO_2$ particle. The electron transfer from CdS to the conduction band of $TiO_2$ increases the charge separation and eventually increases the

efficiency of the photocatalytic process. These separated electrons and holes are then become free to undergo electron transfer with adsorbates on the surface. The experimental results show that coupling of the semiconductors with the appropriate energy levels can produce a more efficient photocatalyst via better charge separation [31, 32].

### 1.6.4) Surface Sensitization

Surface sensitization of a wide band-gap semiconductor photocatalyst such as $TiO_2$ via chemisorbed or physisorbed dye can increase the efficiency of the excitation process. The photosensitization process can also expand the wavelength range of excitation for the photocatalyst through excitation of the sensitizer followed by charge transfer to the semiconductor [33]. Some common dye which are used as sensitizers include erythrosin B [34], thionine [35] and analogs of Ru $(byp)_3^{2+}$ [36]. If the oxidative energy level of the excited state of the dye molecule with respect to the conduction band energy level of the semiconductor is favorable (more negative) then the dye molecule can transfer the electron to the conduction band of the semiconductor. The surface acts as a quencher accepting an electron from the excited dye molecule. The electron in turn can be transferred to reduce an organic acceptor molecule adsorbed on the surface.

# CHAPTER 2

## RATIONALE AND RESEARCH OBJECTIVES

During the past decade, great interest has been focused on a promising technology based on the oxidation of the hazardous and refractory organic compounds, by the use of advanced oxidation processes (AOPs) [37]. The AOPs are based on the generation of hydroxyl radicals ($OH^{\cdot}$) which are the principal agents responsible for the oxidation of numerous aqueous organic contaminants [38,39,40]. Relative oxidation power of some oxidizing species is shown in the table below. Only fluorine gas has a higher electronegative oxidation potential than hydroxyl radical, but it is not used in water treatment (Table 2.1).

**Table 2.1**: Comparison of oxidation power of different oxidizing species [38]

| Oxidation species | Oxidation potential, eV |
|---|---|
| Fluorine | 3.06 |
| Hydroxyl radical | 2.80 |
| Oxygen (atomic) | 2.42 |
| Ozone | 2.08 |
| Hydrogen peroxide | 1.78 |
| Hypochlorite | 1.49 |
| Chlorine | 1.36 |
| Oxygen (molecular) | 1.23 |

Photocatalysis, an AOP, is a rapidly growing field of research with a high potential for a wide range of industrial applications, which includes mineralization of organic pollutants, disinfection of water and air, production of renewable fuels, and organic syntheses. That is why it is called “the treatment processes of the 21st century”.

In recent years, the photocatalytic degradation of various kinds of organic and inorganic pollutants using semiconductor powders as photocatalyst has been extensively studied [41]. This method has been suggested in environmental protection due to its ability to oxidize the organic and inorganic substrates [42]. Semiconductors are particularly useful as photocatalyst because of a favorable combination of electronic structure, light absorption properties, charge transport characteristics and excited-states lifetimes [1]. Surface area and surface defects play an important role in the photocatalytic activity of metal-oxide nanostructures, as the contaminant molecules need to be adsorbed on to the photocatalytic surface for the redox reactions to occur. The higher the effective surface area, the higher will be the adsorption of target molecules leading to better photocatalytic activity.

As discussed in chapter 1.3, various kinds of semiconductor photocatalysts such as $TiO_2$, ZnO, CdS, ZnS, $Fe_2O_3$, $WO_3$ etc. could be used as a photocatalyst. Among them, widely used semiconductor photocatalysts are $TiO_2$ and ZnO. Owing to its relatively high photocatalytic activity, biological and chemical stability, low cost, non-toxicity, and long-term stability against photocorrosion and chemical corrosion, $TiO_2$ has been widely used as photocatalyst [43,44]. However, the photocatalytic activity of the $TiO_2$ (band gap of anatase $TiO_2$ is 3.2 eV) is limited to UV region because $TiO_2$ can only be excited by photon with wavelengths below 387 nm. Due to this reason, effective utilization of solar

energy is limited to about 3-5 % of the total solar spectrum. Also, another problem associated with its application is the fast recombination of photogenerated electron-hole pairs.

ZnO, a traditional n-type semiconductor has been widely used as a photocatalyst owing to its high activity, low cost, and environmentally friendly features. Since ZnO has almost the same band gap energy ( 3.2 eV ) as $TiO_2$, its photocatalytic activity can be anticipated to be similar to that of $TiO_2$. The biggest advantages of ZnO in comparison with $TiO_2$ are that it absorbs over a large fraction of the UV spectrum and the corresponding threshold of ZnO is 425 nm [45]. For this reason, ZnO is the most suitable semiconductor photocatalyst for the photocatalytic degradation (PCD) in the presence of sunlight.

In the case of ZnO, photocorrsion frequently occurs with the illumination of UV light, and this phenomenon is considered as one of the main reasons for the decrease in photocatalytic activity (PCA) in aqueous solutions. However, some studies have confirmed that ZnO exhibits greater photodegradation efficiency (PDE) of some model dyes even in aqueous solution than $TiO_2$ [46]. In the literature, it can be found many comparative studies dealing with the photocatalytic efficiency (PCE) of pollutants over $TiO_2$ and ZnO which have emphasized the effectiveness of ZnO [47-51]. For example, Lizama et al. reported the photocatalytic decolorization of Reactive Blue 19 (RB-19) in aqueous solutions containing ZnO or $TiO_2$ as a photocatalyst and concluded that ZnO is more efficient photocatalyst than $TiO_2$ [47]. Daneshvar et al. reported that ZnO is suitable alternative to $TiO_2$ for the degradation of Acid Red 14, an azo dye [48].

There are still problems that need to be addressed in its application, such as the fast recombination of photo-generated electron-hole pairs. Therefore, improving photocatalytic activity (PCA) by surface modification has become an important topic among researchers in recent years [52-56]. One approach is to dope transition metals into ZnO, and the other is to form coupled photocatalyst [57-61]. Recently, it was found that substitution of a non-metallic element such as nitrogen, phosphorus, sulfur, carbon etc. for oxygen in the ZnO lattice is more efficient in improving its PCA [62-68]. Doping of metal ions, such as $Al^{3+}$, $Cu^{2+}$, $Fe^{3+}$, etc., has been widely employed to enhance the PCA of ZnO [69-72]. Zheng et al. reported that Ag deposited on ZnO surface exhibits improve PCA by suppressing the recombination of charge carriers [73,74]. The reason for increase in PCA is that the noble metal Ag acts as a sink for photogenerated electron. They also reported that the PCA of Ag/ZnO photocatalyst depends on the dispersion of Ag particles in the photocatalyst and the photocatalyst particles in the dye solution. The higher the dispersions of metallic Ag in Ag/ZnO photocatalyst and Ag/ZnO catalyst in the dye solution were, the higher the PCA of Ag/ZnO photocatalyst should be. L. R. Zheng et al. have showed that $SnO_2$/ZnO synthesized through a two-step solvothermal method exhibited excellent PCA compared to individual components of $SnO_2$ and ZnO. Such a mechanism was also supported by the study of Kundu et al. on nanoscale ZnO/CdS heterostructures prepared by wet chemical route for Methylene Blue (MB) photodegradation [75].

As explained in chapter 1.6.4, sensitization of a wide band gap semiconducting material such as ZnO and $TiO_2$ with dyes has been used to improve the PCA [76-78]. The sensitization process is primarily limited by the relative positions of the conduction band

(CB) of the wide and narrow band gap semiconductor and also the nature of the interfaces in the system [79, 80]. While the first factor could be controlled by the appropriate choice of material and by tuning the band gap of the sensitizer [81], the second factor still remains challenge in terms of creating a favorable interface/heterojunction in order to facilitate facile electron transfer. Recently, many groups have attempted creating efficient heterojunctions for CdS- $TiO_2$ and CdS-ZnO [81-84] using different methods but high PCA was achieved in only a few cases [85].

Moreover, C. Shifu et al. [86] found that p-n junction photocatalyst p-NiO/n-ZnO prepared by sol-gel method showed enhance activity compared to individual components and their physical mixture for the photodegradation of methyl orange (MO), a model dye. Such a mechanism was also supported by the study of Hameed et al. [87] on NiO-ZnO nanocomposites prepared by co-precipitation/co-gel techniques for the photodegradation of rhodamine B (RB) and study of Z. Zhang et al. [88] on p-NiO/n-ZnO nanofiber heterojunction prepared by facile electrospinning technique for the phothodegradation of RB. Furthermore, Li et al. [89] reported that hierarchical-structure ZnO-CuO nanocomposite (NC) prepared by one-step homogeneous coprecipitation method showed a higher PCA than the monocomponent oxides and their physical mixture. This was mainly attributed to the extended photo-responding range towards visible light and the increased charge separation rate in nanocomposite.

However, all the above explained strategies (surface modification and optimization of solar energy which are explained in details in chapter 1.6) have had only limited success and, therefore the development of new materials is of paramount importance. As explained in earlier paragraphs, ZnO is a widely used traditional n-type semiconductor

( Eg = 3.37eV ) photocatalyst due to presence of oxygen vacancies. On the other hand, CuO is a p-type transition metal oxide with a narrow band gap ( Eg = 1.85 eV ). This CuO possesses high p-type concentration, high hole mobility, and low lattice mismatch with ZnO, which is beneficial for the formation of p-n heterojunction with ZnO [90,91]. Therefore, p-CuO/n-ZnO nanocomposite was selected as a target material to synthesize by using a simple ball milling technique.

In the process of ball milling, the crystal lattices of the ZnO and CuO undergo severe plastic deformation, producing stresses and strains. This creates a crystal lattice distortion, while at the same time forming many defects inside particles. Such defects have surface energy and lattice distortion energy. This makes the activation energy for diffusion of elements decrease significantly, and allows for atomic or ionic marked diffusion among elements at room temperature. When the activity of the powder system is high enough, during the ball milling process, the collision between balls and grains of the powder will produce a rise in the interface temperature, which will generate the coupled system [92]. So, when the interface of p-CuO and n-ZnO contact each other, the p-n junction nanocomposite photocatalyst p-CuO/n-ZnO can be formed. It is expected that p-n junction nanocomposite of 1D ZnO and CuO nanomaterials exhibits novel photocatalyst due to the improved junction potential between ZnO-CuO, which helps in efficient $e^-/h^+$ pair charge separation upon excitation.

The n-n type composite photocatalyst, such as $ZnO/TiO_2$, $SnO_2/ZnO$, $SnO_2/ TiO_2$ and $WO_3/ TiO_2$, and so on have been investigated extensively. However, the study of the p-n type composite photocatalyst is limited. Theoretically, when p-type semiconductor CuO and n-type semiconductor ZnO form p–n junction, the inner electric field will be

formed at the interface. At the equilibrium, the inner electric field makes p-type semiconductor CuO region have the negative charge, while ZnO region have the positive charge. Under near UV illumination, electron-hole pairs may be created, and the photogenerated electron-hole pairs are separated by the inner electric field. The holes flow into the negative field while the electrons move to the positive field. As a result, the photogenerated electrons and holes are separated efficiently, and the PCA is enhanced.

It is known from the heterogeneous photocatalytic mechanisms that the quantum efficiency of the photocatalytic reaction depends upon two key processes: one is the competition between the recombination and capture of photogenerated electrons and holes; the other one is the competition between the recombination of captured electrons and holes and interface charge transfer. The lengthening recombination time of electrons and holes and increasing interface electron transfer rate are both favorable for the enhancement of the quantum efficiency. Therefore, in order to increase the quantum efficiency of photocatalytic reaction, the recombination of the photogenerated electron-hole pairs must be decreased.

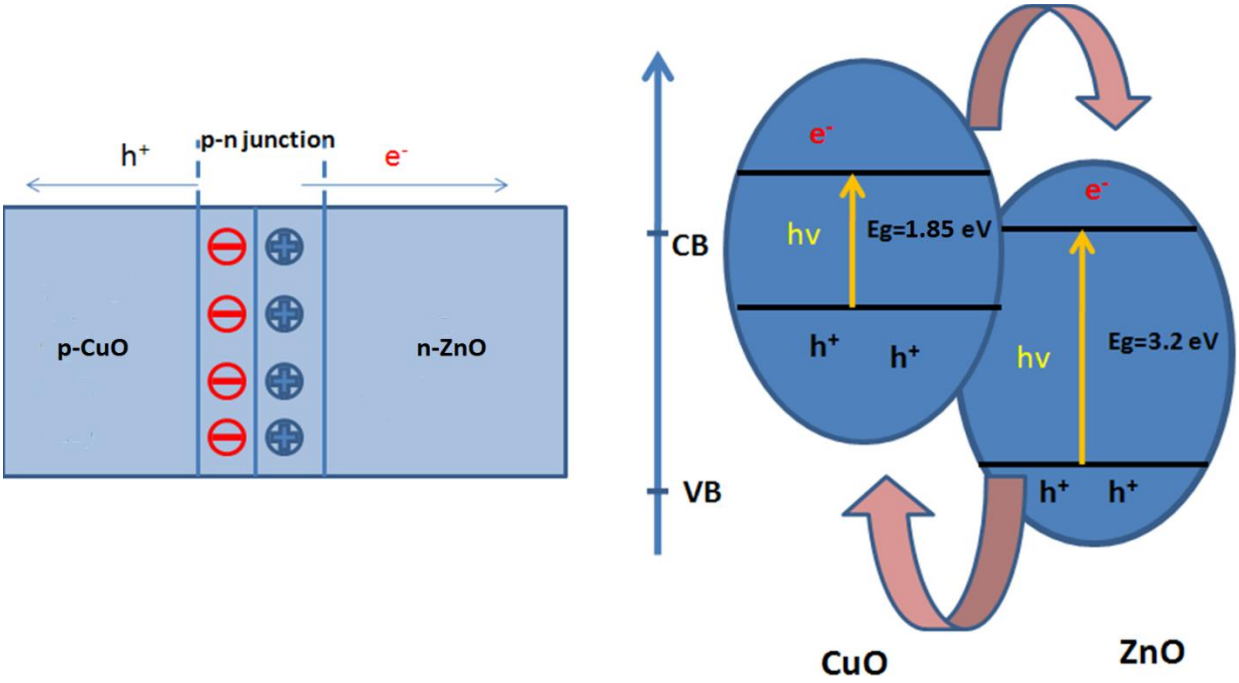


**Figure 2.1**: A p-n junction formation model and a schematic diagram of photoexcited electron-hole separation process under visible light and UV light irradiation.

Figure 2.1 depicts the p-n junction formation model and the schematic diagram of electron-hole separation process on the surface of a CuO-ZnO sample. When p-type CuO and n-type ZnO integrate, many micro p-n junction CuO/ZnO photocatalyst will be engendered at the interface of the CuO and ZnO nanoparticles. At equilibrium, an electric field forms that makes the CuO p-type semiconductor region have negative charges while the ZnO region have positive charges. The electron hole pairs will be created under UV light irradiation. With the effect of the inner electric field, the holes flow into the negative field and the electrons move to the positive field. Therefore, the photogenerated electron-hole pairs will be effectively separated by the p-n junction formed in the interface of

CuO/ZnO [93]. The efficient charge separation could increase the lifetime of the charge carriers and enhance the efficiency of the interfacial charge transfer to adsorbed substrates and then account for the higher activity of the p-type CuO and n-type ZnO heterojunction nanocomposite.

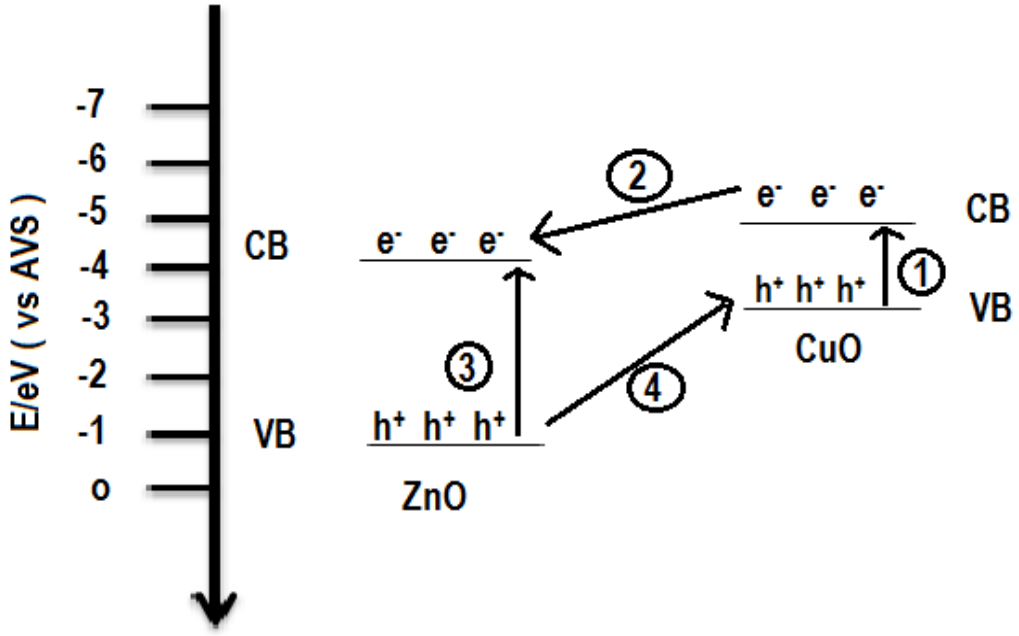


**Figure 2.2**: Energy band diagram of the CuO/ZnO composite system, showing corresponding valence and conduction band positions.

The enhanced PCA of the CuO/ZnO composite system both under UV and UV-Vis irradiation of light can be interpreted using the schematic diagram of energy band structure of the system as shown in Fig 2.2. Under irradiation of light both CuO and ZnO can be excited according to process (1) and (3), respectively. The conduction band (CB)

edge of CuO (-4.96 eV vs. absolute vacuum scale (AVS)) is higher than that of ZnO (-4.19 eV vs. AVS); the valence band (VB) of edges of CuO and ZnO are situated at -3.26 eV and -0.99 eV vs. AVS, respectively [Am. Miner, 85 (2000)]. From thermodynamic point of view, the photogenerated electron transfer from CB of CuO to that of ZnO, while the photodegenerated holes immigrate in the opposite direction i.e. from the VB of ZnO to that of CuO. It is important to note that under visible light illumination, the interband transition of electron within CuO i.e. process (1) still occurs, on the other hand ZnO cannot be activated due to its broad band-gap i.e. process (3) does not take place.

The photocatalytic mechanism of the experiment is proposed as follows:

$$\text{(p-type CuO/n-type ZnO)} + h\nu \xrightarrow{\text{under UVlight}} e^-(\text{ZnO}) + h^+(\text{CuO})$$

$$e^- + O_2 \rightarrow O_2^{\cdot -}$$

$$h^+ + OH^- \rightarrow OH^{\cdot}$$

$$O_2^{\cdot -} + H_2O \rightarrow HO^{\cdot}_2 + OH^-$$

$$HO^{\cdot}_2 + H_2O \rightarrow H_2O_2 + OH^{\cdot}$$

$$H_2O_2 \rightarrow 2OH^{\cdot}$$

$$OH^{\cdot} + MB \rightarrow CO_2 + H_2O$$

Under UV light irradiation, the photogenerated electrons moved to the ZnO side whereas holes moved to the CuO side. Afterward, the holes were trapped by surface hydroxyl group (or $H_2O$) to yield $OH^{\cdot}$ radicals. The dissolved oxygen molecules reacted with the electrons to yield superoxide radical anions, $O_2^{\cdot -}$, which on protonation

generated the hydroperoxy, $HO_2^{\cdot}$, radicals, producing hydroxyl radical $OH^{\cdot}$, which was a strong oxidizing agent for decomposing the organic dye [94,95].

Since various parameters affect the photocatalytic activity of the photocatalyst. Some of them are:

- Substrate (MB) concentration
- Concentration of photocatalyst in the reaction solution
- pH value
- Particle size
- Concentration of Wt. % of CuO in nanocomposite (ZnO-CuO)
- Calcination time of photocatalyst
- Heat treatment time of photocatalyst

In the present study, all these issues are systematically addressed.

# CHAPTER 3

# EXPERIMENTAL PROCEDURES AND CHARACTERIZATION TECHNIQUES

## 3.1) Materials Used in the Experiment

ZnO (crystallite size of about 50-56 nm) and CuO (size about 30-35 nm) powders used in the experiment were purchased from US Research Nanomaterials Inc. Chemical used to adjust the pH of the suspensions to a desire value are HCl or NaOH solutions. Deionized water was used throughout this study. For UV light irradiation throughout the experiment, mercury UV lamp (Oriel Corporation, Model 68810, wavelength 436 nm G-line) of power 200-500 W was used. Methylene Blue (MB), a potent model dye, used throughout the experiment was purchased from Acros Organics (purity 99.9%). The structure of MB (molecular formula $C_{16}H_{18}ClN_3S$ ) is shown below for reference.

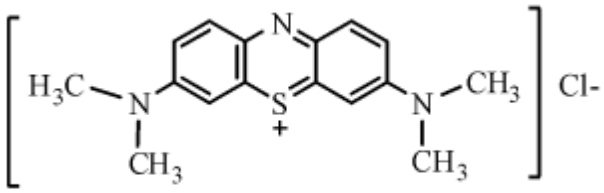


methylene blue (MB)

Table 3.1: Percent composition of MB (tetramethylthionine chloride) by element

| Element | Symbol | Atomic Mass | # of Atoms | Mass Percent |
|---|---|---|---|---|
| Chlorine | Cl | 35.453 | 1 | 11.084% |
| Hydrogen | H | 1.00794 | 18 | 5.672% |
| Carbon | C | 12.0107 | 16 | 60.081% |
| Nitrogen | N | 14.0067 | 3 | 13.137% |
| Sulfur | S | 32.065 | 1 | 10.025% |

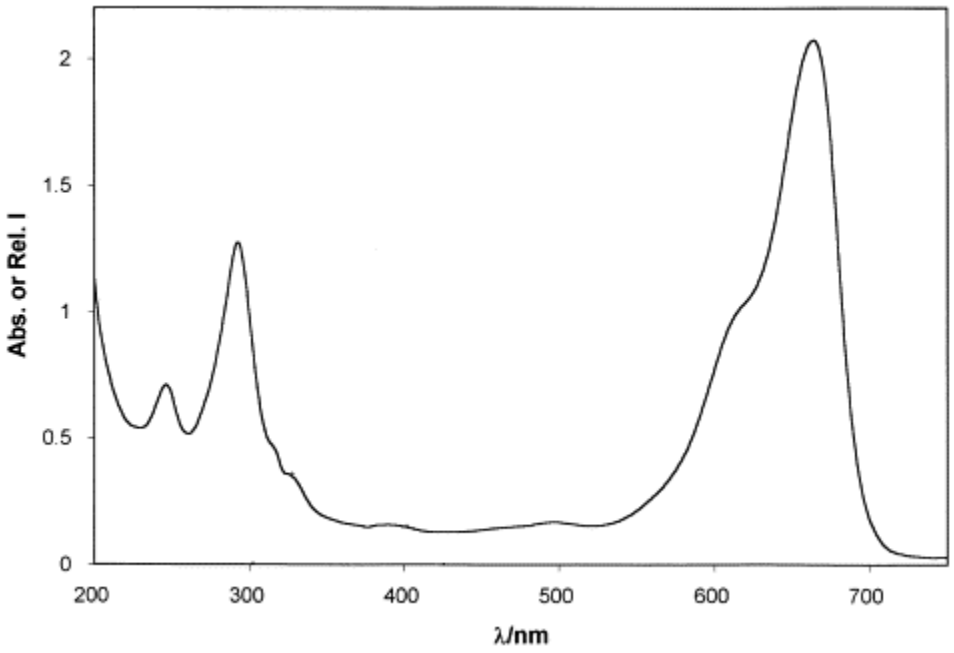


**Figure 3.1**: UV-Vis absorption spectra of MB.

### 3.2) Synthesis of Composite Materials

Various methods have been used for the synthesis process. Some widely used methods are wet chemical route, solid state reaction, sol-gel, mechanically mixing, ball milling etc.

### 3.3) Synthesis Procedures

#### 3.3.1) Synthesis of temperature dependent samples

ZnO (size 50-56 nm) and CuO (size 30-35 nm) powders were measured in equal proportion. The two samples were then mixed with deionized water (dispersant) and ball milled was carried out in a planetary ball mill (Fritsch Planetary ball mill). The rotational speed was set to 400 rpm with powder to ball weight ratio 1:10 for 20 hours. The wet composite sample was dried at 110 $^{o}$C for 3h in air. Samples were then divided into four samples and heated at varying temperature of 200, 400, 600 and 800 $^{o}$C to initiate crystalline growth. Pure ZnO and CuO NPs were also heated at above temperature for the comparison. The as-prepared calcinated samples were used for the PCA characterization. The flow chart of synthesis of temperature dependent samples is as shown in Scheme 3.1.

#### 3.3.2) Synthesis of varying CuO concentration samples

CuO (x, Wt%)/ZnO, composite with x= 1, 5, 10, 15, 20, 30, 40, and 50 were synthesized via mechanical grinding. ZnO (crystallite size of about 50-56 nm) and CuO (size about 30-35 nm) powders used in the experiment were purchased from US Research Nanomaterials Inc. The preparation of of p-CuO/n-ZnO photocatalyst was carried out in a planetary ball mill (Fritsch Planetary ball mill) using deionized water as dispersant at 400 rpm with powder to ball weight ratio 1:10 for 12 hours. The samples were also grinded

for additional hours up to 72 hours. The wet powder was dried at 110 $^{0}$C for 3h in air and was used for the PCA characterization.

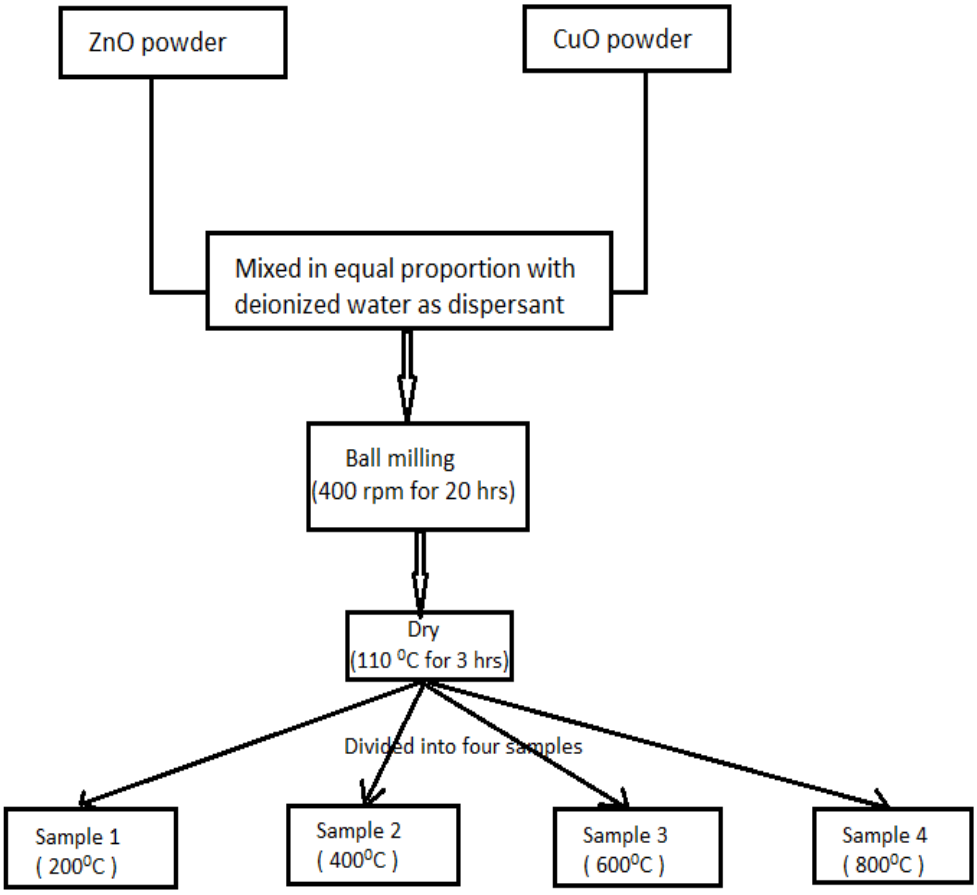


**Scheme 3.1**: The flow chart of preparation of calcined CuO-ZnO samples

### 3.4) Photocatalysis Tests

To examine the photocatalytic activity of the prepared samples, photodegradation of methylene blue (MB), a popular test contaminant, was investigated. 0.005 gm of MB was dissolved in 1 liter of deionized water by ultrasonicating the solution from 10-15 min.

The photocatalytic activity experiments were carried out by adding ~ 10 mg of as-prepared samples into 50 mL of the MB solution. The suspension was stirred in the dark for 10 min to obtain the saturated adsorption of MB before illumination of UV light source. This solution was exposed to a 200-500 W mercury UV lamp (Oriel Corporation, Model 68810, wavelength 436 nm G-line). The mixture was exposed to UV light in 5 min intervals. The concentration change of MB was determined by monitoring the optical intensity of absorption spectra of MB at 291 nm via Ocean Optics UV-Vis spectrometer in a transmission mode. The photodegradation efficiency of photocatalyst was calculated by using following expression:

$$\eta = \frac{C_O - C_t}{C_O} \times 100\%$$

Where η is the photocatalytic efficiency; $C_0$ is the concentration of reactant before illumination; $C_t$ is the concentration of reactant after illumination time t.

## 3.5) Characterization Techniques

### 3.5.1) Structural Characterization

Structural analysis of the as-prepared samples such as particle size, morphology of the particle was studied by using X-ray diffraction (XRD), and, transmission electron microscope (TEM).

#### 3.5.1.1) X-ray Diffraction (XRD)

X-ray diffraction is used to determine the crystal structures by interpreting the diffraction patterns formed when x-ray are scattered by the electron of atom in crystalline solids. X-rays are sent through a crystal to reveal the pattern in which molecules and atoms contained within the crystal are arranged.

In XRD, a powder of crystalline sample is irradiated with a monochromatic beam of X-ray, and the beam is diffracted as Bragg's law. A detector records the diffracted beam as a pattern. The intensity and Bragg's angle determine the characteristics of the crystal. Crystallite size and crystal phase composition of as-prepared samples were determined by using Bruker Advance D8 x-ray diffractometer with Cu $K_\alpha$ radiation ($\lambda$=1.54056 Å).

Firstly, samples were deposited on a zero background (Si) sample holder and then the x-rays were sent to them. In our study, the diffraction patterns were observed at room temperature within the range of 2θ angle from 20-75 $^0$. Thus obtained x-ray patterns were matched with the standard pattern from ICCD database.

To determine the crystal size of the nanoparticle, the full width half maxima and the twice the diffraction angle were noted. The following Scherrer's equation is used [96]:

$$D = \frac{0.89\lambda}{\beta \times Cos\theta}$$

Where 'D' is the average crystallite size of the particle, 'λ' is the wavelength of the Cu $K_\alpha$ radiation (λ=1.54056 Å), 'θ' is the Bragg's angle of diffraction, and 'β' is the full width at half maxima.

### 3.5.1.2) Transmission Electron Microscope (TEM)

The transmission electron microscope works under high energy electron beam transmitted through a very thin sample to image and analyze the microstructure of materials with atomic scale resolution. The electrons are focused with electromagnetic lenses and the image is observed on a fluorescent screen, or recorded on film or digital camera. TEM forms an image by way of differential contrast. Those electrons that pass through the sample go on to form the image while those that are stopped or deflected by dense atoms in the specimen are subtracted from the image. In this way, a black and white image is formed.

While examine the specimen inside the TEM, two extreme conditions such as high vacuum and intense heat generated by the beam of electron have to be taken into consideration. For this reason, specimen has to be reasonably dried and thin for ensuring electron transparency. TEM images were obtained by using JEOL JEM-1200EX, which

was operated an accelerating voltage of 120 kV and can magnify the images up to 500K. For the preparation of sample, very little amount of sample was dispersed in deionized water by sonication about 20 minutes. The well dispersed solution was dropped on the carbon coated copper grid by the use of pipette. The grid was left for several hours to make the specimen free from water.

### 3.5.2) Surface Characterization

#### 3.5.2.1) Zetasizer Nano ZS (Malvern)

Malveren Zetasizer Nano ZS can be used to measure the zeta potential and particle size of nanomaterial samples in aqueous solutions. The zeta potential of a particle is the overall charge that the particle acquires in a particular medium which can be studied as a function of the pH value. Particle surface characteristics and charge play an important role in the particle's physical state, stability in different media, agglomeration tendencies, and interaction with biological systems. Zeta potential measurement provides an indirect measure of the net charge and as a tool to test batch-to-batch consistency. The magnitude of the measured zeta potential is an indication of the repulsive force that is present and can be used to predict the long-term stability of the product. If all the particles in suspension have a large negative or positive zeta potential then they will tend to repel each other and there is no tendency for the particles to come together. However, if the particles have low zeta potential values then there is no force to prevent the particles coming together and flocculating.

In zeta potential measurements, an electrical field is applied across the sample and the movement of the particles (electrophoretic mobility) is measured by the light

scattering of the particles. The Henry equation is then used to calculate the zeta potential, *z*:

$$U_e = \frac{2\varepsilon z f(\kappa a)}{3\eta}$$

Where '$U_e$' is the electrophoretic mobility, 'ε' is the dielectric constant, η is viscosity of the medium, *f* (*ka*) is the Henry function, and *ka* is a measure of the ratio of the particle radius to the Debye length. Electrophoretic determinations of zeta potential are most commonly made in aqueous media and moderate electrolyte concentration. *f* (*ka*) in this case is 1.5, and this is referred to as the Smoluchowski approximation.

To prepare the sample for Zeta Potential, very small amount of sample was well dispersed in deionized water by using ultrasonic disruptor (an effective tool for dispersing NP in aqueous solution) for 20 minutes. The pH value of the suspending medium was controlled to the desire value by using NaOH or HCl. The solution was stirred continuously to observe the effect of the NaOH or HCl into the solution and the pH value. At least three runs were performed for each zeta potential measurement for the conformity of the measurement.

### 3.5.3) Optical Characterization

#### 3.5.3.1) UV-Vis Spectrometry

In UV-Vis spectrometry, a beam of light from a visible and/or UV light source is passed through a small transparent container (cuvette) containing a solution under study. Many molecules absorb ultraviolet or visible light. But different molecules absorb radiation of different wavelengths and have different absorption intensities. Ultraviolet-visible (UV-Vis) spectrometer records the absorbance of the sample solution under study for particular wavelength of radiation. Beer's law states that, 'absorbance is directly proportional to path length and concentration of the absorbing species' and is given by

$A = \varepsilon bc$

Where ε is the constant of proportionality, b is the path length, and c is the concentration of absorbing species [97].

UV-Vis study was carried out by using Ocean Optics Spectrometer in the range of 200-800 nm. Light was blocked by using black sample to save as a dark spectrum and deionized water was used as a reference sample. For this purpose, disposable sterile plastic cuvettes were used.

# CHAPTER 4

# RESULTS AND DISCUSSION

## 4.1) Structural Characterization

XRD was used to investigate the phase structure and average crystallite size of the p-n junction photocatalyst CuO/ZnO.

### 4.1.1) XRD studies

Figure 4.1 shows the X-ray diffraction (XRD) patterns of CuO (50%)/ZnO photocatalyst prepared at different heat treatment temperatures (200, 400, 600, 800 $^{o}$C). The reaction time was fixed as 5h. From figure, it is clear that, the characterization diffraction peaks of the prepared photocatalyst are connected with heat treatment temperature. It is obvious from figure that, the higher the heat treatment temperature is, stronger the diffraction peaks and the narrower the peaks become. This indicates that with the increase of heat treatment temperature, the crystal become perfect, and some crystal grains agglutinate and become bigger.

Crystallite sizes of the of p-n junction photocatalyst CuO (50%)/ZnO were calculated by putting full-width-at-half-max and Bragg's angle values in Scherrer's formula [96]. It can be seen from the inset of the figure 4.1 that the crystallite size of the ZnO and CuO in the CuO (50%)/ZnO photocatalyst increases with the heat treatment increasing from 200 to 800 $^{o}$C. Similar results have reported by Shifu et al. in their study of p-NiO/n-ZnO [100].

Figure 4.2 shows the XRD pattern of p-CuO (x, Wt%)/n-ZnO powders ball milled for 12 hours. All the peaks were clearly identified as monoclinic CuO or hexagonal wurtzite ZnO. The diffraction peaks of both constituent of the composite are well defined, revealing the well-crystalline character of the samples. No other impurity phase was detected in the composite.

Powder x-ray diffraction patterns of CuO (wt. 10%)/ZnO photocatalyst ball-milled time 12, 24, 36, 48, 60, and 72 hours is as shown in figure 4.3. From the search-match database analysis, it is confirmed that all the peaks in the patterns are either due to ZnO or CuO. This analysis revealed that impurities were not formed during the ball milling process. The crystallite size of ZnO in the CuO (10 Wt.%)/ZnO composite milled for different milling time is also shown in the inset of Fig 4.1. Average crystallite size of ZnO in the composite was calculated by x-ray line broadening analysis using Scherer's formula [96]. It can be seen that the particle size decreases with the increase in ball milling time.

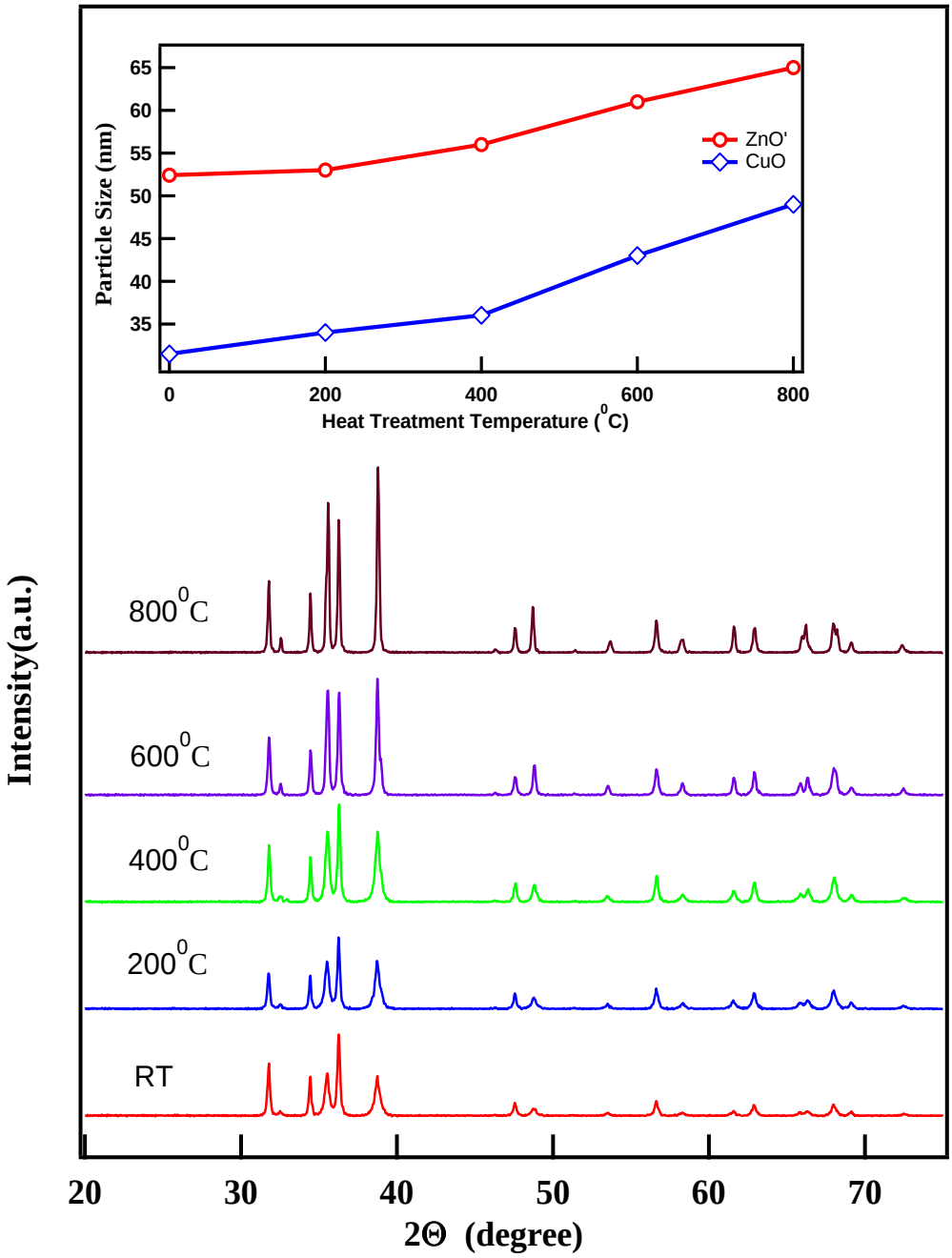


**Figure 4.1**: XRD patterns of CuO (50%)/ZnO sample heated at various temperatures for 5 hours. The inset shows the effect on particle size due to heat treatment temp.

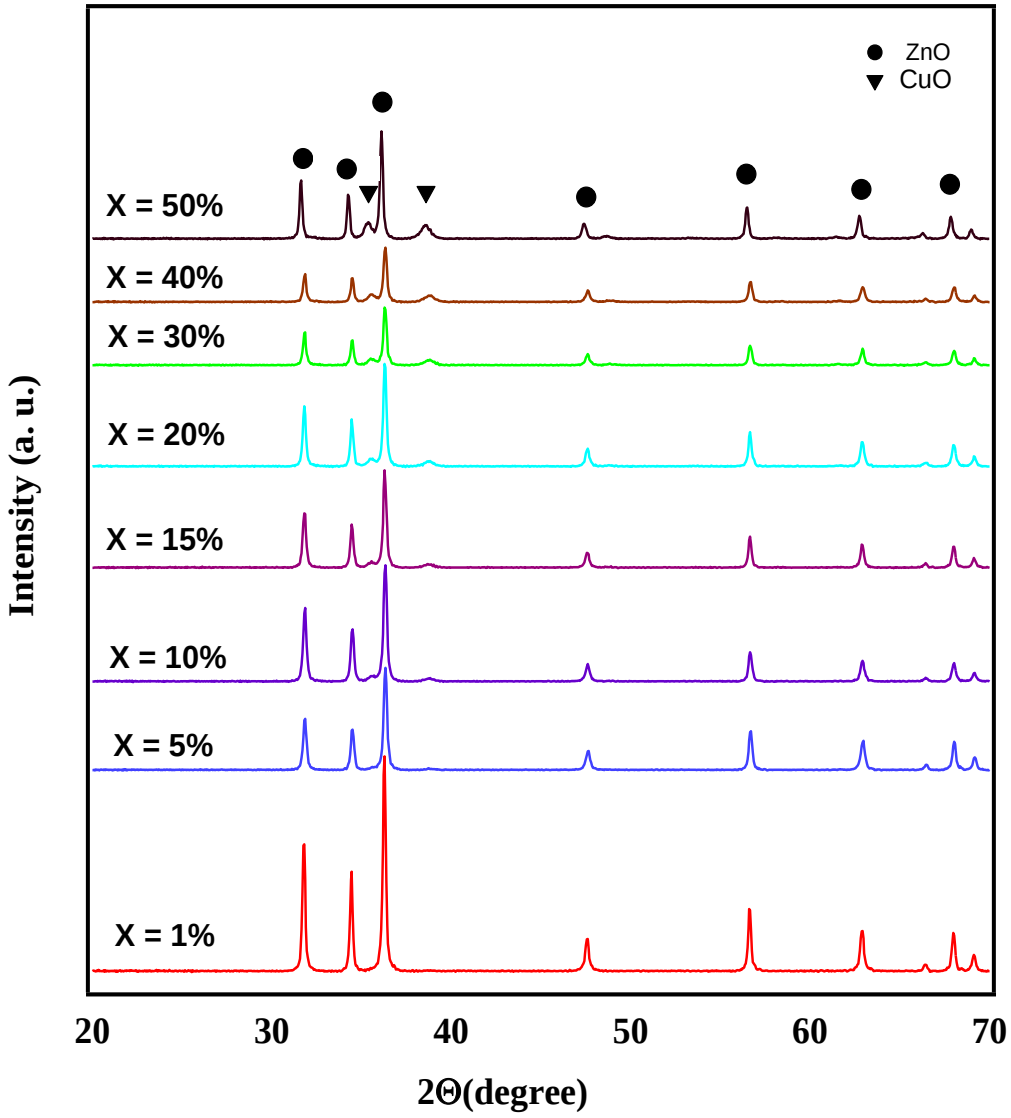


**Figure 4.2**: XRD patterns of various wt% of CuO samples: CuO (x, Wt%)/ZnO (x = 1, 5, 10, 15, 20, 30, 40, and 50) ball milled 12 hours.

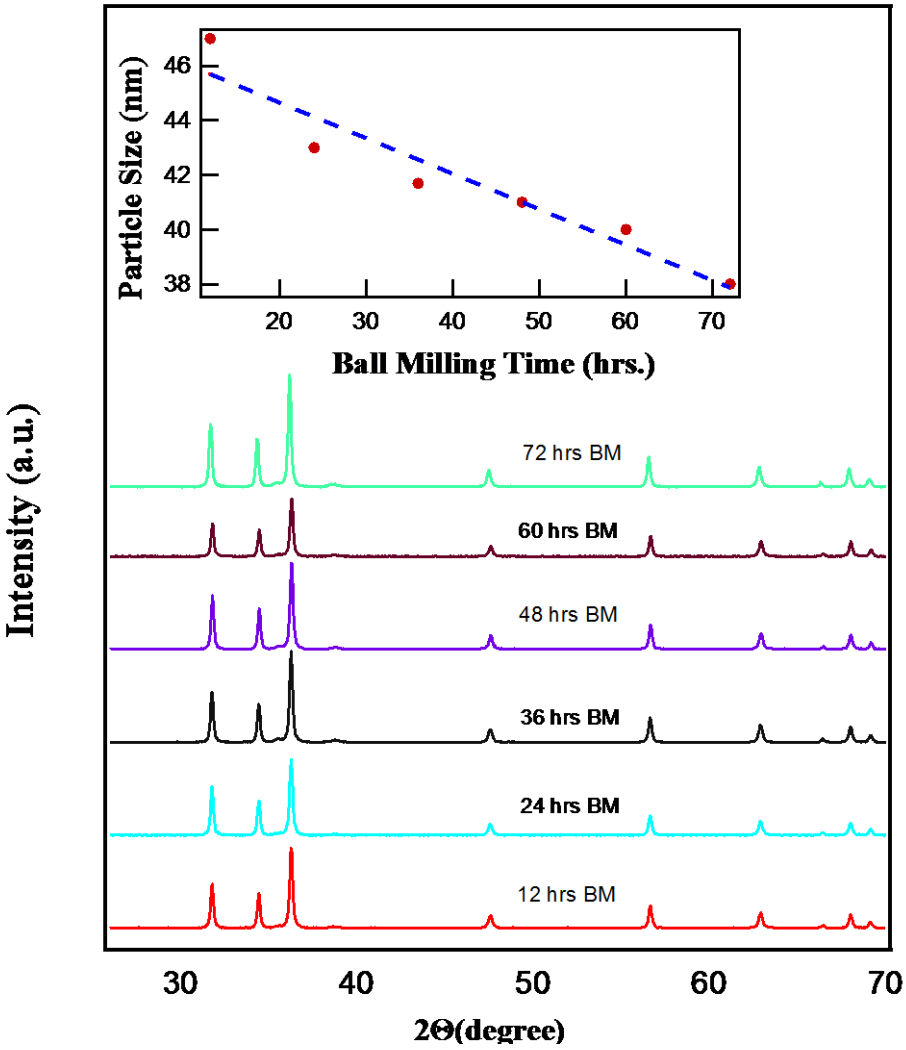


**Figure 4.3**: XRD patterns of CuO (wt. 10%)/ZnO photocatalyst ball-milled for different hours. The inset shows the effect on particle size as a result of ball milling time.

### 4.1.2) TEM Studies

TEM was used to investigate the morphology and to calculate the average particle size of the samples. In order to investigate the interface of the sample, CuO (Wt. 10%)/ZnO ball milled 12 hours was chosen for TEM and high-resolution TEM characterization.

Figure 4.4 gives an overview of the typical TEM image of the CuO (Wt. 10%)/ZnO photocatalyst. It clearly exhibits the existence of CuO nanoparticles with mean size of about 30-35 nm dispersing over the particle Of ZnO. It is also observed that the dispersion degree of sample ball milled for 12 hours is higher than of the sample ball milled for 36 hours. When the ball milling time is longer than the optimum time the fresh surfaces formed by the high energy ball milling possesses high surface energy and prefer to agglomerate. Similar result was reported by Wei et al. in their p-CuBi2O4/n-TiO2 photocatalyst study [101]. They reported that sample ball milled for 6 hours showed higher dispersion degree.

Figure 4.5 shows the TEM micrographs of p-n junction photocatalyst CuO (Wt. 50%)/ZnO calcined at 600 $^0$C for 5 hours. The average particle size calculated for ZnO and CuO were about 62 and 44 nm respectively. It can be seen that the particle size of ZnO and CuO in p-n junction photocatalyst CuO/ZnO calcined at 400 $^0$C had smaller particle size (about 57 nm for ZnO and 37 nm for CuO). By contrast, the p-n junction photocatalyst CuO/ZnO calcinated at 800 $^0$C showed greater particle size (about 66 nm for ZnO and 50 nm for CuO). This indicates that increase of heat treatment temperature caused p-n junction photocatalyst CuO/ZnO particles to become larger. The result was in agreement with that of the XRD. It also clearly specified that the surface areas of the p-n

junction photocatalyst CuO/ZnO decreases with the increase of heat treatment temperature.

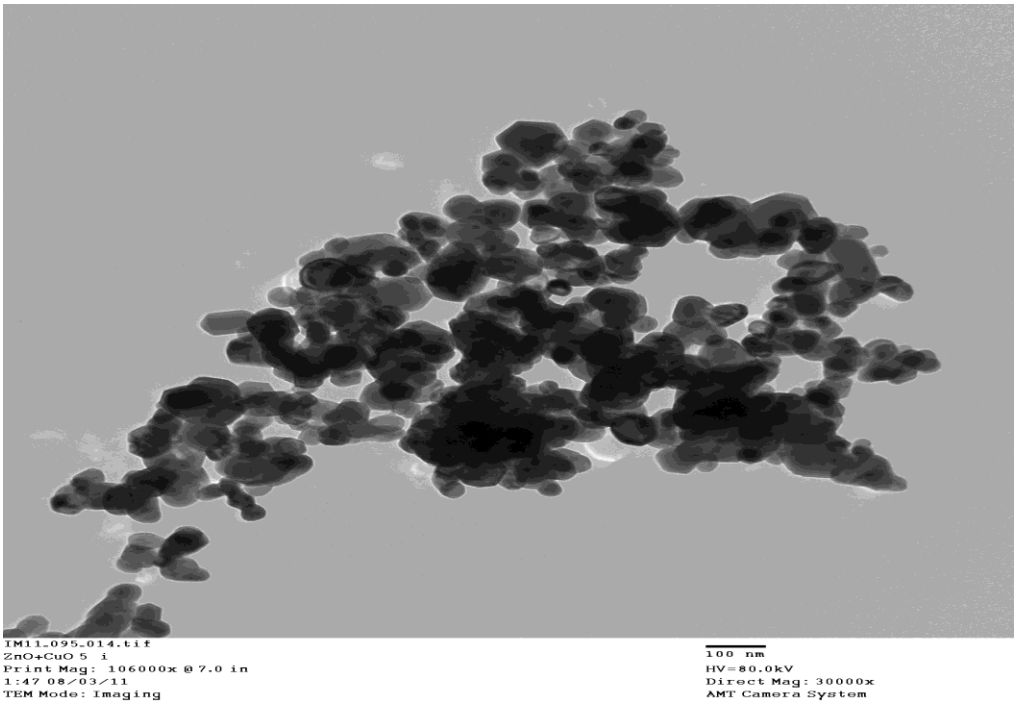


**Figure 4.4**: TEM images of 12 hours ball milled CuO (Wt. 10%)/ZnO sample.

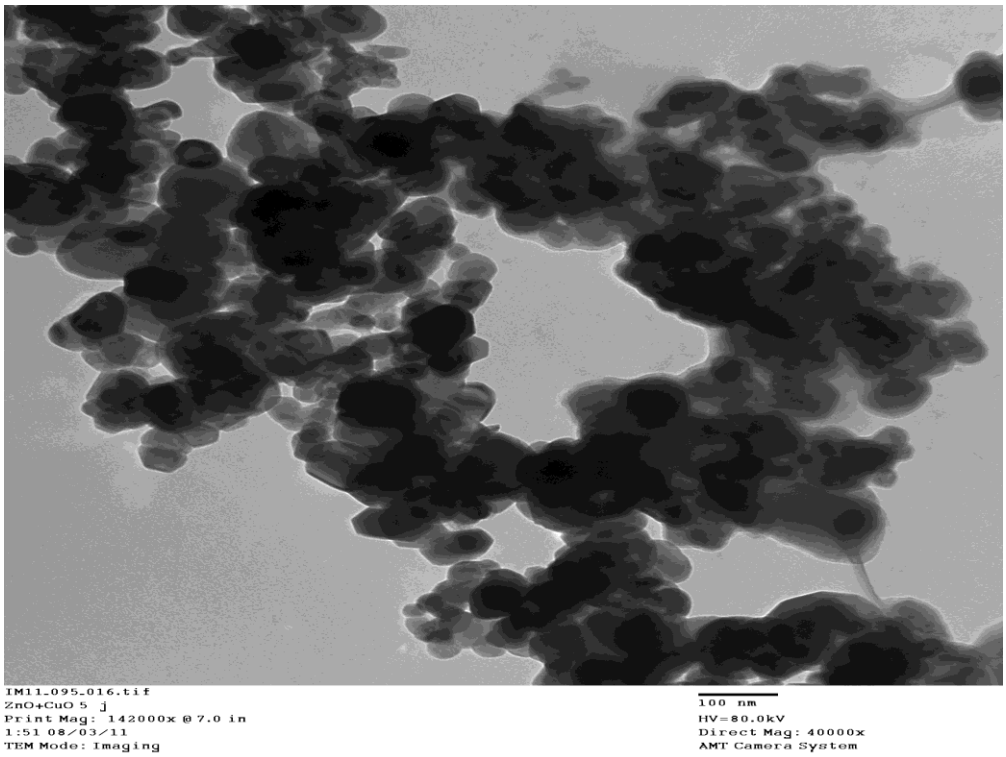


**Figure 4.5**: TEM images of CuO (Wt. 50%)/ZnO photocatalyst calcined at 600 $^{o}$C.

## 4.2) Optical Characterization

In order to investigate the optical properties of the as-prepared samples optical studies were performed by using UV-Vis Spectroscopy.

### 4.2.1) UV-Vis analysis

In order to investigate the photocatalytic activity (PCA) properties of the photocatalyst, UV-vis absorption study of Methylene blue (MB) was conducted as a function of UV exposure time in the presence of CuO/ZnO composite. The concentration of MB was estimated from the UV-vis peak of MB at 291 nm. Figure 4.6 shows the UV-Vis MB spectra recorded in the presence and absence of composite as a function of UV

exposure time. The degradation rate constant of MB was determined from the first-order kinetic equation $-\ln(C_o/C)=kt$, where $C_o$ is the initial concentration of MB and C is the concentration of MB after UV exposure in the presence of sample for time "*t*", and "*k*" is the rate constant. From the Figure 4.6, it is clear that the MB peak intensity decreases with the UV exposure time in the presence of composite powder. This observation clearly illustrates the role of CuO/ZnO as a photocatalyst.

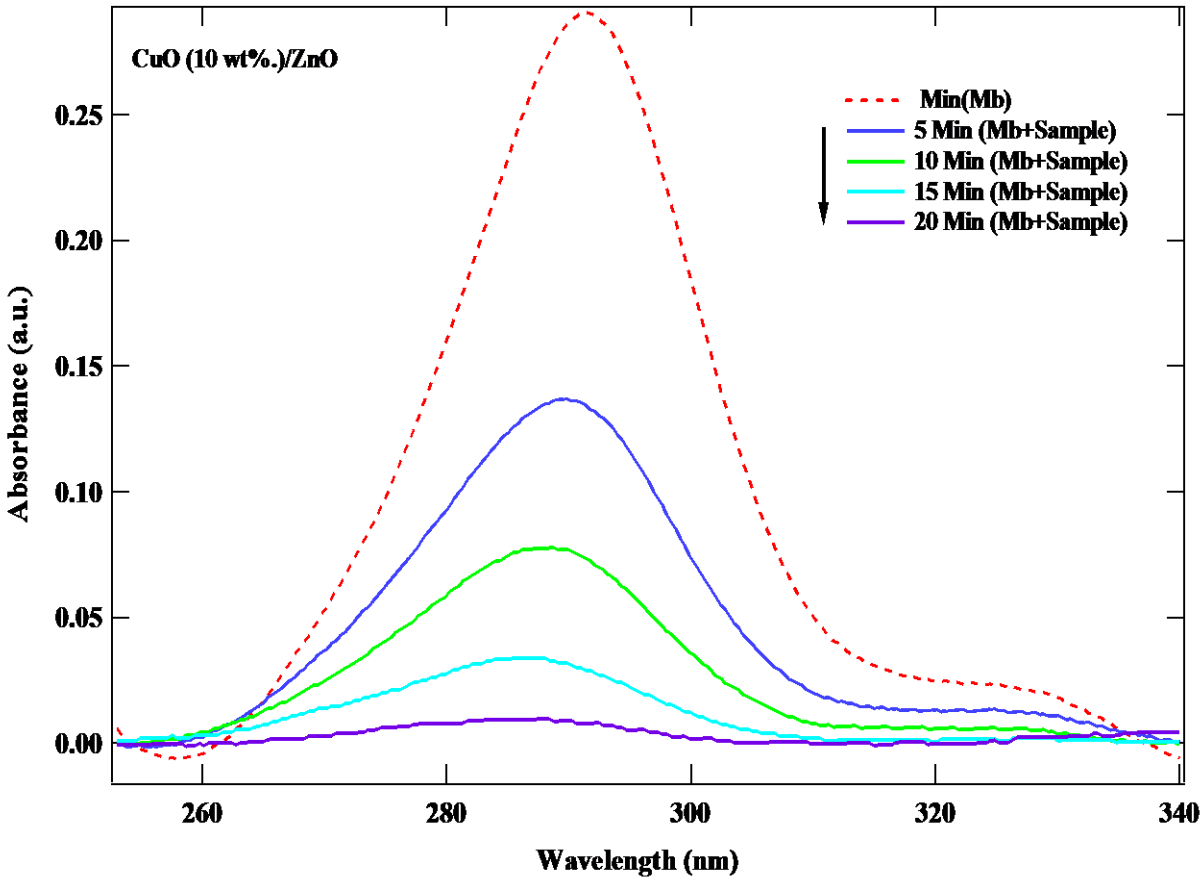


**Figure 4.6**: Photodegradation of MB in the presence of 12 h ball milled Cu (10 wt%)/ZnO sample.

### 4.3) Studies of various parameters that influence on PCA

Parameters that influence the PCA of the photocatalyst were studied to obtain highly efficient novel photocatalyst.

#### 4.3.1) Effect of calcination temperature on PCA of photocatalyst

In order to evaluate the effect of calcination temperature on photocatalyst, PCA were performed under UV light radiation using calcined samples. UV-Vis MB spectra recorded in the presence and absence of calcined samples as a function of UV exposure time. The degradation rate constant of MB was determined from the first-order kinetic equation.

Figure 4.7 shows the comparative rate constant study ZnO, CuO, and CuO (Wt. 50%)/ZnO photocatalysts as a function of heat treatment time. It can be seen from figure that catalytic activity decreases with the increase of the calcination temperature. From figure it is clear that, catalytic activity of CuO (Wt. 50%)/ZnO photocatalyst lies in between ZnO and CuO photocatalyst. The decrease in photocatalytic activity of the calcined CuO (Wt. 50%)/ZnO sample may be due to the grain growth of individual components. The grain growth increases the migration time for electron and hole to reach the surface leading to decrease in photocatalytic activity. Thus from heat treatment process, the catalytic activity of the composite photocatalyst cannot be exceeded than the catalytic activity of monocomponent ZnO. The particle size of the calcined samples were calculated by x-ray line broadening analysis using Scherer's formula and found that particle size increases (shown in the inset of figure 4.1) significantly with the increase of heat treatment temperature. This indicates that, the higher the heat treatment temperature

is, larger the particle size and the lower the surface area become. In addition, it also suggests that catalytic performance not only depends on surface area and the morphology but also depends on the particle size and crystallinity. Increasing temperature decreases the solubility of $O_2$ and thus decreases the concentration of photogenerated holes, thus lower the degradation rate. The high temperature calcination of photocatalyst will result in the removal of surface hydroxyl groups, which are the strong oxidizing agents for the removal of organic pollutant [102].

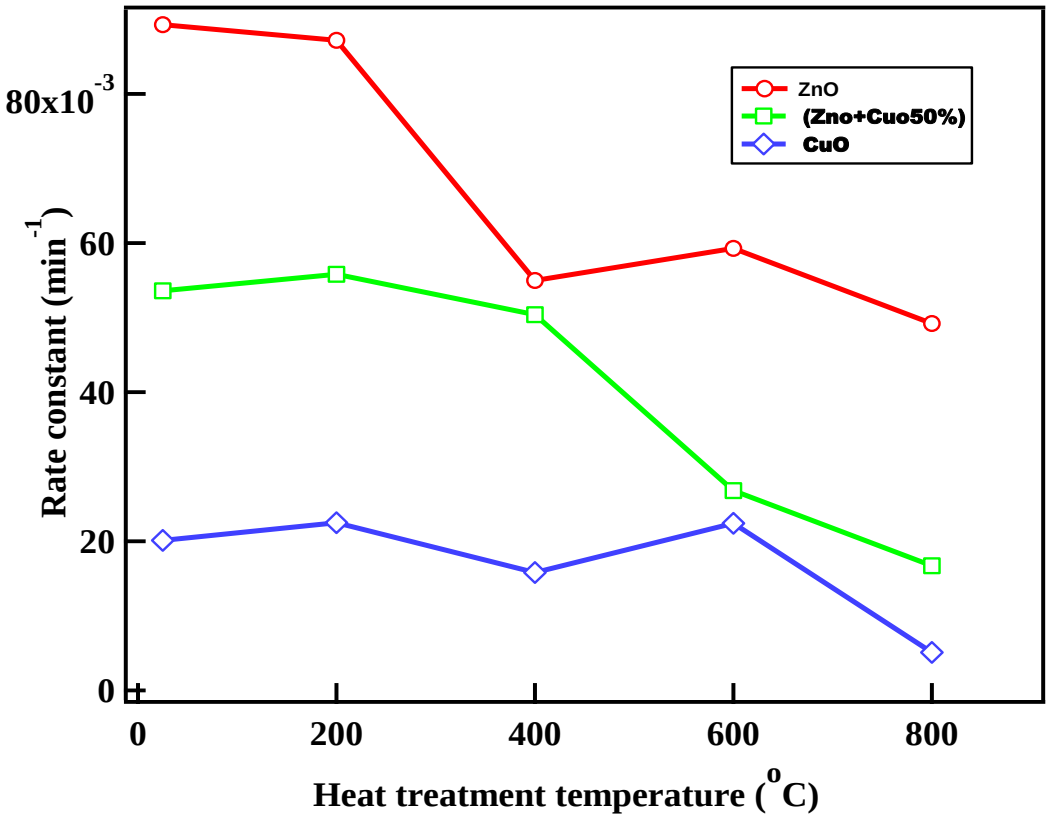


**Figure 4.7**: Comparison rate constant of ZnO, CuO, and CuO (Wt. 50%)/ZnO photocatalyst as a function of heat treatment temperature.

### 4.3.2) Effect of CuO Wt.% in the composite on the PCA

In order to evaluate the effect of Wt.% of p-CuO on the p-n junction p-CuO/n-ZnO photocatalyst, PCA were performed under UV radiation using samples ball milled for 12 h. The experiment was carried out using composites of different Wt.% of p-CuO from 0% to 50 wt%. The rate constant evaluated for the series of samples is shown in the Fig 4.8.

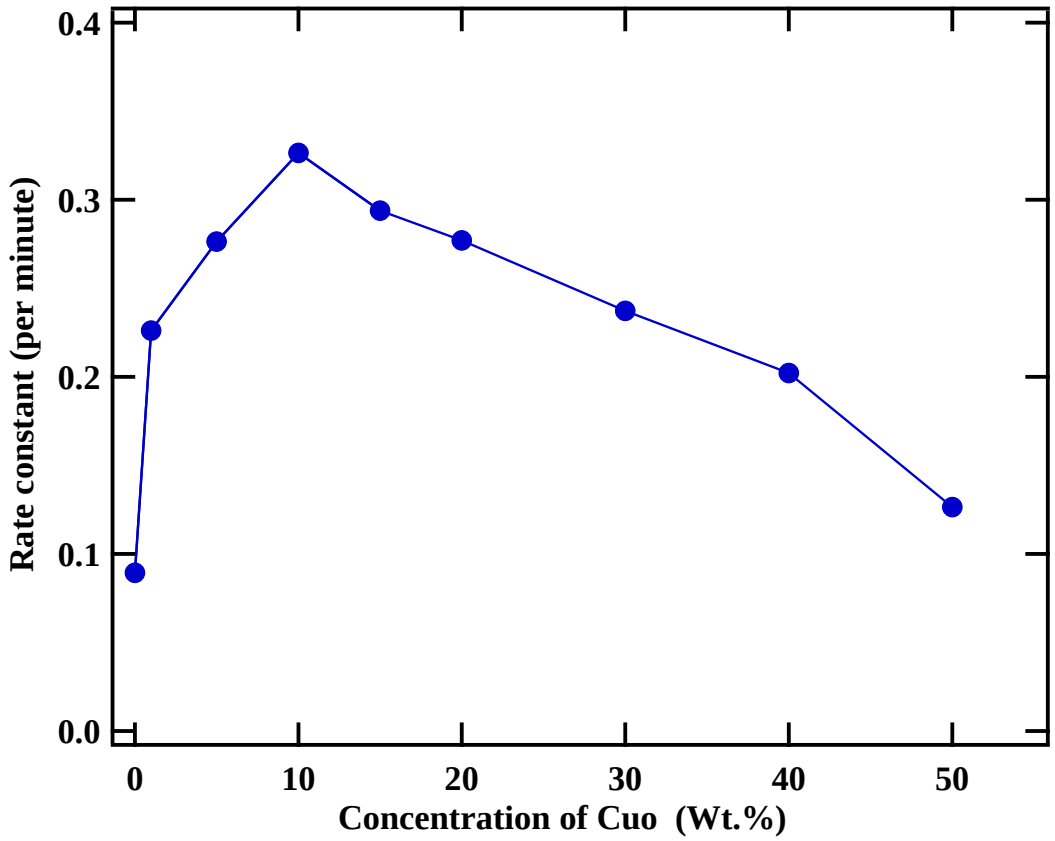


**Figure 4.8**: Rate constant vs. concentration of CuO in as prepared nanocomposites photocatalyst.

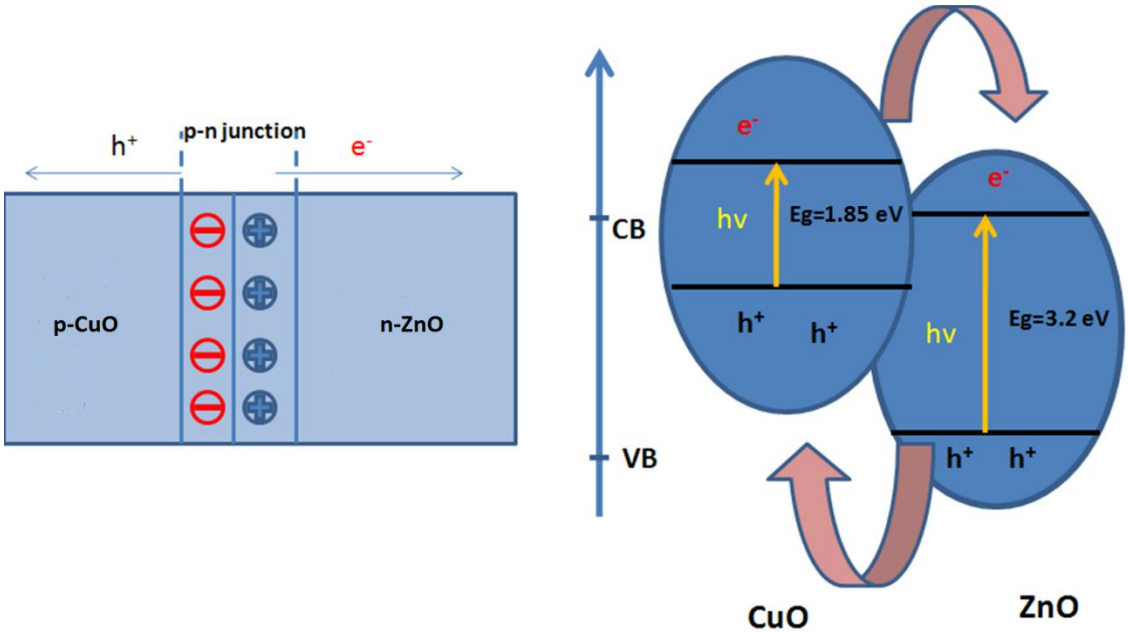


**Figure 4.9**: A p-n junction formation model and a schematic diagram of photoexcited electron-hole separation process under visible light and UV light irradiation.

From Fig 4.8, it can be seen that the wt.% of p-CuO plays an important role in the photocatalytic degradation of MB. The photocatalytic activity of p-CuO/n-ZnO is much higher than that of pure ZnO under UV light irradiation. The photocatalytic activity increases remarkably with the increase in concentration of p-CuO in the composite from 0% to 10 wt%. Under UV light irradiation, when the amount of p-CuO is 0%, namely pure ZnO, the rate constant is 0.0893 $min^{-1}$ (particle size ~53 nm) and degradation efficiency 94%. When the amount of p-CuO increases from 0% to 10 wt% photocatalytic degradation increases rapidly from 94% to 99% and rate constant reaches a maxima, 0.3265 $min^{-1}$. However, for p-CuO amount exceeding 10 wt.%, gradual decrease in PCA

is observed. The possible reasons for the increased PCA of the p-n junction photocatalyst at low concentration of p-CuO in the composites are as follows: When the p-type CuO and n-type ZnO integrate, p-n junction will be formed between p-CuO and n-ZnO, and the junction potential will be formed at the interface [103]. At the equilibrium, the inner electric field makes p-type CuO region negatively charged while n-type ZnO positively charged. The electron-hole pairs are created under the UV light illumination. Due to the presence of junction potential, the holes flow into the negative field whereas electrons move to the positive field. In this way, photogenerated electron-hole pairs will be separated effectively by the p-n junction formed in the p-CuO/n-ZnO. This efficient separation of charge carriers, make these charges readily available for photooxidation of MB thus leading to PCA enhancement. The schematic diagram for the above explanation is illustrated in Fig 4.9.

Furthermore, under UV light irradiation, the energy of the excitation light is large enough to excite both the p-CuO and ZnO. As shown in Fig 4.9, the photoexcited holes produced in the ZnO valence band will transfer to the valence band of the p-CuO particle, while the electron generated in the p-CuO conduction band will transfer to the conduction band of the ZnO particle. At the same time, the photogenerated electron of ZnO will remain in the conduction band of ZnO, which makes charge separation more effective. The separated electrons and holes are then free to undergo reactions with adsorbates on the photocatalytic surface. Therefore, photocatalytic degradation can be enhanced with the increasing concentration of p-CuO due to the increase in the number of the separated electrons and holes [104,105].

It is proposed that, when the amount of CuO is lower than the optimum amount, the increase of the amount of CuO can increase trapping sites of the carriers, which prolongs the lifetime of the carriers, thereby improving the photocatalytic activity. More importantly, an addition of small amount of CuO can prevent the growth of the ZnO granule, and this made specific surface area of the photocatalyst increases, so the PCA increases. But when the amount of p-CuO is higher than 10 wt%, photocatalytic activity decreases gradually. This is because when the amount of p-CuO is higher than the optimum amount of doping, the high concentration dopant ions act as recombination centers of electrons and holes, decrease the thickness of the space-charge layer on the surface of ZnO particle, and reduce the photon absorption [106]. On the other hand, the results also showed that p-CuO powder had almost no photocatalytic activity under UV light irradiation, whereas ZnO did. This indicates that, when the p-CuO is higher than its optimum amount of coupling, the photocatalytic activity decreases. The result is further verified by the zeta potential measurement.

### 4.3.3) Effect of substrate concentration on PCA

It is an important both from a mechanistic and an application point of view to study the dependence of substrate concentration on the photocatalytic reaction rate. As the redox reaction proceeds, less and less of the surface of the photocatalyst particle is covered as the pollutant is decomposed. The decrease in photocatalytic rate is to be expected with the increasing irradiation time and the rate of degradation becomes zero when the pollutant is completely decomposed or the reactant solution becomes clear.

Figure 4.10 shows the plot of degradation rate constant of CuO (Wt. 10%)/ZnO photocatalyst as a function of MB weight. The effect of the substrate concentration by the

use of CuO (Wt. 10%)/ZnO photocatalyst was studied at different weights of substrate (MB) such as 0.7, 1.25, 2.50, and 3.75 mg. Here it is interesting to note that rate constant increases with the increase in substrate weight from 0.7 to 1.25 mg and further increase in substrate weight from 1.25 to 3.75 mg leads to decrease in rate constant. Similar results have reported by Minero et al. in their study of degradation of phenol [107]. Qumar et al. have also reported the same kind of trend in their study of degradation of vanillin [108]. The possible explanation for this behavior is that as the concentration of model pollutant such as MB increases, more and more molecules of the compound get adsorbed on the surface of the photocatalyst, therefore the requirement of crystal surface needed for the degradation also increases. In this study, the generation of relative amounts of $OH^{\bullet}$ and $O^{\bullet}_{2}{}^{-}$ on the surface of the catalyst does not increase as the intensities of light, illumination time and the amount of catalyst were kept constant. Consequently, photocatalytic reaction of the photocatalyst decreases as the concentration increases.

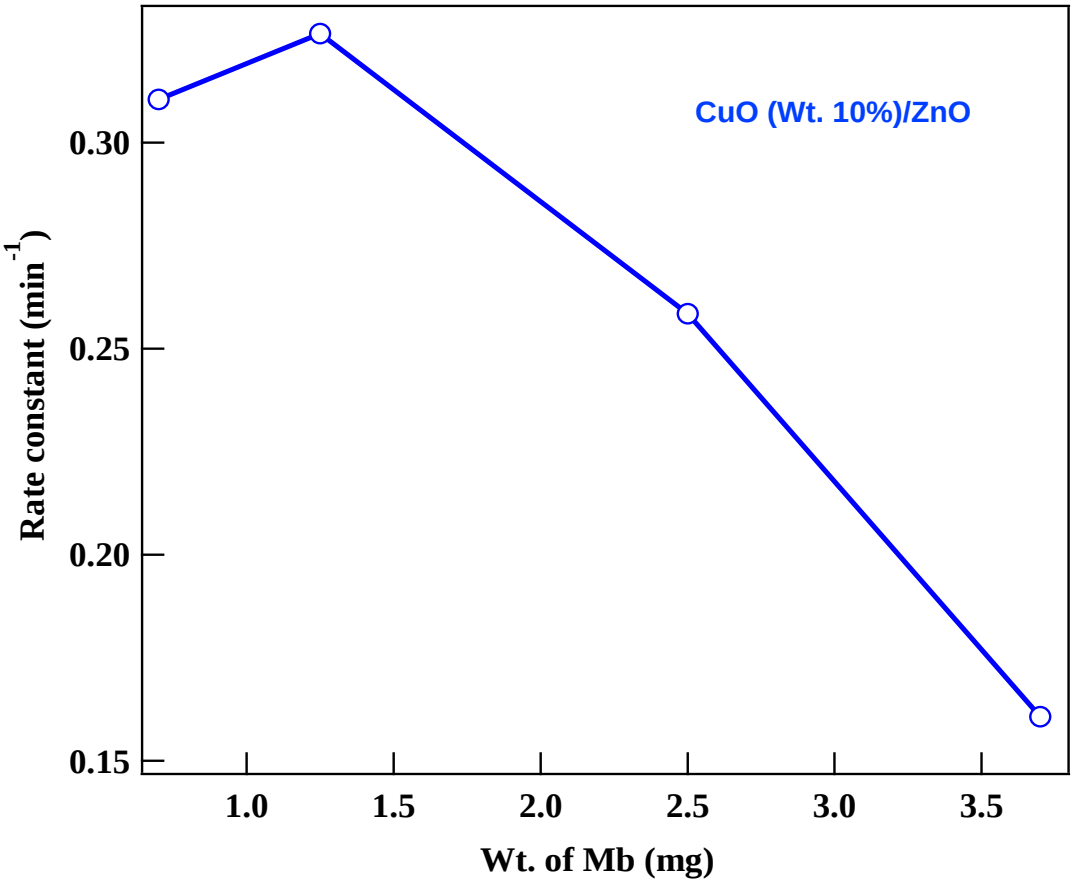


**Figure 4.10**: Rate constant as a function of MB weight for 12 h ball milled CuO (wt.10%)/ZnO sample.

### 4.3.4) Effect of pH on the PCA

An important parameter in the photocatalytic reactions taking place on the particulate surfaces is the pH of the solution. Since it dictates the surface charge properties of the photocatalyst and the size of aggregates it forms. So, the solution pH is an important variable in the evaluation of aqueous phase mediated photocatalytic reactions [109]. In order to evaluate the effect of the pH on the p-n junction CuO (Wt. 10%)/ZnO photocatalyst, PCA were performed. The effect of pH was studied by keeping all other experimental conditions constant and changing the initial pH value of the MB

solution from 3 to 10 and results are shown in Fig 4.11. pH of the MB was adjusted to the desire value by dilute HCl or KOH solution. Since the charge and surface potential are primarily pH dependent those influence the PCA, so the adjustment of pH to the desire value is expected to enhance the photocatalysis reaction. If the surface charge of the particle is high enough, a stable suspension without the formation of hard agglomerates is prepared [110,111].

Figure 4.11 illustrates the effect of pH on the PCA of CuO (Wt. 10%)/ZnO photocatalyst. It can be seen from figure that rate constant increases with the increase in pH value of MB and reaches to its maximum value at pH 7.1; rate constant is 0.3265 $min^{-1}$. As shown in the figure, the value of rate constant decreases on increasing the pH value of MB beyond 7.1. This phenomenon could be attributed to the instability or photocorroding behavior of ZnO under acidic condition (pH at or lower than 5). The dissolution of CuO (Wt. 10%)/ZnO photocatalyst may be due to a classical chemical process of ZnO. It is now widely recognized that dissolution plays an important role in PCA. The mechanism describing the dissolution of ZnO under extreme acid/base conditions has been demonstrated in literature [112]. It was found to be mainly influenced by pH as well as the specific surface area of the nanoparticles. The dissolution rate of ZnO nanoparticle was found moderate at pH 6 and 8 [112]. And the rate was found decrease markedly at pH 7. Therefore, reduce of the PCA of CuO (Wt. 10%)/ZnO at exceeding low and high pH values can originate from dissolution of ZnO at extreme acid/base condition. A similar kind of degradation trend has observed by Akyol et al. and Kaneco et al. in their PCA study of ZnO as a function of pH [113,114].

The result of our study indicates that pH value of the solution was a key factor to dye degradation and changing the pH value of the solution affects the degradation efficiency of the photocatalyst significantly. Therefore, the best reaction pH value for the photodegradation of MB was chosen as 7.

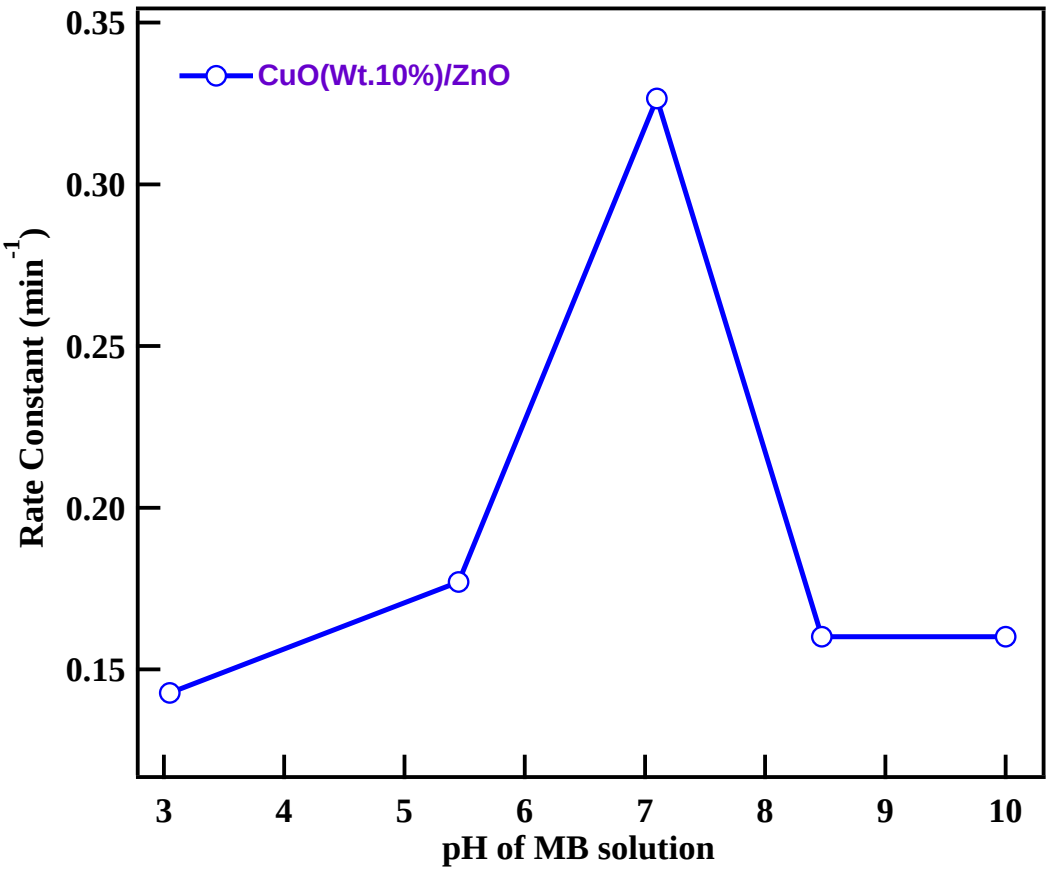


**Figure 4.11**: Effect on the PCA of 12 h ball milled Cuo (wt. 10%)/ ZnO photocatalyst as a function of pH.

### 4.3.5) Effect of photocatalyst concentration on PCA

Figure 4.12 shows the effect of concentration of photocatalyst on the PCA. It can be seen that concentration of the photocatalyst influences the overall PCA. The effect of

concentration of photocatalyst for the photodegradation of MB was studied by keeping all other experimental parameter constant and changing the weight of the sample from 7 to 16 gm and results are illustrated in Fig 4.12. The parameters which were kept constant thorough out the study are as follows: volume of MB solution 50 ml, pH value ~7, weight of the MB 1.25 mg.

It can be seen from figure that rate constant increases with the increase in concentration of the photocatalyst for the photodegradation of MB solution. This result was expected, it is the characteristic of heterogeneous photocatalysis to increase the degradation efficiency with the increase in concentration of the photocatalyst and this result is in agreement with a number of studies reported earlier [115,116,117]. The reason can be expounded that at lower catalytic loading much of light may be transmitted through the solution. However, higher reaction rates at a higher amount of catalyst loading may be explained in terms of complete utilization of incident photons striking on the catalyst surface i.e., higher adsorption of incident light can lead to the formation of high photoactivated volume in suspension thereby increasing the efficiency of the system [116]. As shown in the figure, the maximum rate constant is found with sample loading 10 mg and the value of rate constant is 0.3265 $min^{-1}$. On further increasing the weight of the photocatalyst , the rate constant decreases gradually. The rate constants calculated for 12.8 and 16 gm of photocatalyst are 0.2967 $min^{-1}$ and 0.2218 $min^{-1}$ respectively. This result indicates that above the certain concentration the reaction rate levels off and becomes independent of the catalyst concentration. Daneshwar et al., for instance, found that the optimum catalyst loading for the best degradation is 160 mg $L^{-1}$ [118]. In another study, the optimum catalyst concentration was found to be 1 g $L^{-1}$ [115]. Many other

examples could be presented here demonstrating the different optimum catalyst loading for different investigations. Moreover, the nature of the model dye under investigation can also affect the optimum catalysis loading [116]. Hence, the optimum loading of catalyst therefore depends on the geometry and working conditions of the photo-reactor, concentration and nature of organic pollutants, and nature of the photocatalyst. When the photocatalyst concentration is very high, after travelling a certain distance on an optical path, turbidity impedes further penetration of light in the reactor lowering the efficiency of the system. Thus from the above study we can conclude that concentration of photocatalyst play a crucial role for the photodegradation of organic pollutants and changing the concentration of photocatalyst into the solution affects the photocatalytic reaction significantly.

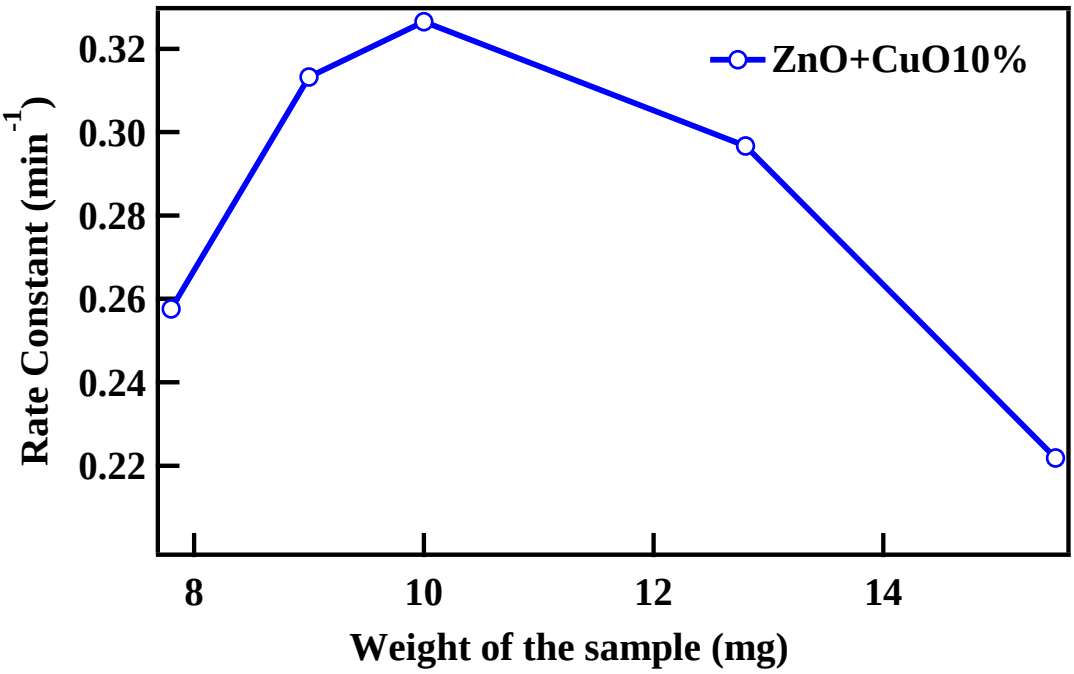


**Figure 4.12**: Rate constant of CuO (Wt. 10%)/ZnO nanocomposite as a function of catalyst weight.

### 4.3.6) Effect of Ball Milling Time on the Photocatalytic Activity

Figure 4.13 shows the effect of ball milling time on the PCA of CuO (10 wt%)/ZnO photocatalyst. It can be seen that the ball milling time influences the photocatalytic activity strongly. It is verified that photocatalytic activity of p-n heterojunction p-CuO/n-ZnO is much higher than that of the mixture of p-CuO-n-ZnO without ball milling [119]. The reason may be attributed to that ZnO and p-CuO only play their own photocatalytic roles without ball milling, and p-n junction heterojunction photocatalyst is not formed. However, ZnO and p-CuO form p-n heterojunction after ball milling. When the ball milling time is 12, 24, 36, 48, 60 and 72 h, the photodegradation efficiency is 99.1, 99.0, 97.9, 98.6, and 98.4 %, respectively. This indicates that PCA of p-n heterojunction 12 hours ball milled CuO/ZnO reach to its maximum with conversion

efficiency of nearly 100% under illumination time of 15 min. The PCA decreases gradually with the increase in the ball milling time as shown in the figure 4.13.

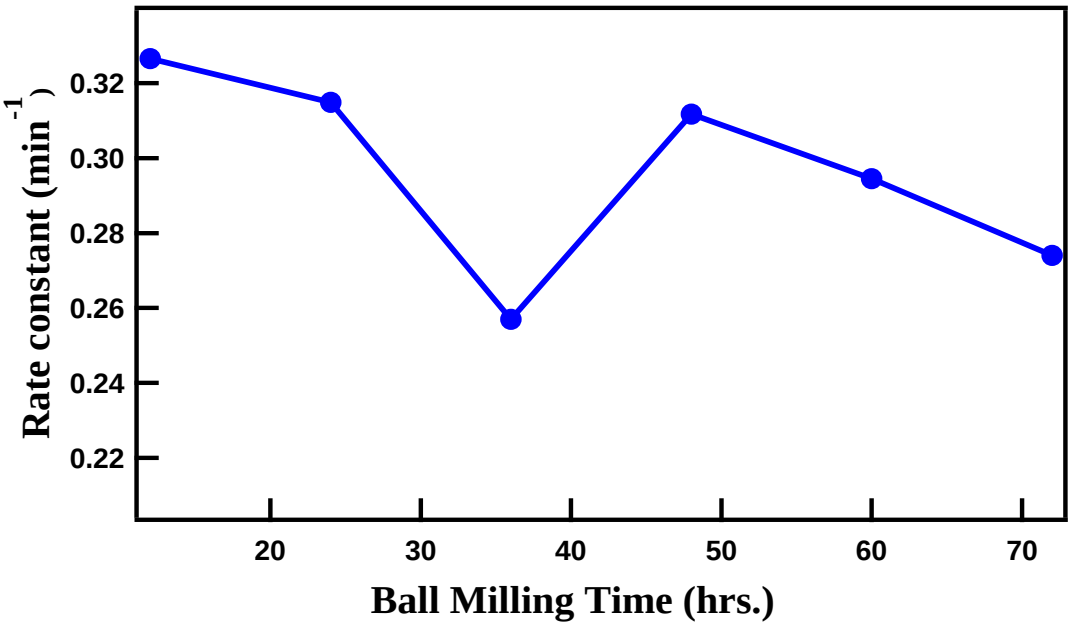


**Figure 4.13**: Photocatalytic rate constant as a function of ball milling time for CuO (10 Wt%)/ZnO photocatalyst.

It is proposed that, when the amount of p-CuO is lower than its optimum amount, with the increase in the amount of CuO, the p-n junction photocatalyst p-CuO/n-ZnO is formed by ball milling, which helps the electron-hole pairs to separate effectively and PCA to enhance. When the ball milling time is 12 h, the effect of separating electron-hole pairs is the best and the PCA is the highest compared to other ball milling time. Similar results have reported for ZnO/$TiO_2$ ball milled samples [120].

Another reason for the best PCA observed for 12 h ball milled samples is that the specific surface area of the photocatalyst must be higher as compared to samples

prepared for other ball milling time. The PCA is highly dependent upon the surface area of particles and usually the powders with high surface area are expected to be good PCA [121]. For samples ball milled up to 12 hours, the number of active sites per unit weight of photocatalyst must be high as has been reported earlier specific surface area study of $ZnO/TiO_2$ [120]. At ball milling times longer than the optimum time, the sample possess high surface energy which prefers to agglomerate [122, 123], resulting in the decrease of the PCA. At the same time, a number of crystal defects and inner $Zn^{2+}$ in the ZnO lattice are produced during high energy ball milling. In addition, the crystal defects and the inner $Zn^{2+}$ will become recombination center for photogenerated electrons and holes [124]. This assumption is further verified by the dependence of zeta potential on ball milling time for CuO (10 Wt.%)/ZnO sample as shown in Fig 4. A continuous decrease in zeta potential with increasing ball milling time evidently shows the increased agglomeration of particles which in turn reduces PCA.

### 4.3.7) Effect of heat treatment time on the PCA

It is known that PCA depends on the heat treatment temperature and heat treatment time of the photocatalysts. Figure 4.14 (b) shows the effect of duration of heat treatment on the PCA of the 12 h ball milled CuO (wt. 10%)/ZnO photocatalyst. The fixed heat treatment temperature was 700 $^oC$ and duration of heat treatment was 3, 4, 5, and 6 hours. From figure 4.14 (b), it is clear that the PCA of CuO (wt. 10%)/ZnO photocatalys gradually increases with the increase in duration of heat treatment from 3 hrs. up to 6 hrs. For a heat treatment of 6 hours, the PCA of CuO (wt. 10%)/ZnO photocatalys reaches to its maximum value, the rate constant is 0.0129 $min^{-1}$. For the duration of heat treatment temperature 3 hours, the value of rate constant is only 0.0028

$min^{-1}$. The value of rate constant is increased by 360 % with the increase in heat treatment duration from 3 to 6 hrs. The possible reason may be due to improvement in the crystallinity of the sample with increase in heat treatment time. Therefore, the longer heat treatment time exhibits an advantageous effect on the PCA. Shifu et al. have reported the similar result in their study of NiO/ZnO photocatalyst [100].

The growth of the ZnO particle as a function of heat treatment for CuO (wt. 10%)/ZnO photocatalyst is as shown in Fig 4.14(a). Average crystallite size of ZnO in the composite was calculated by x-ray line broadening analysis using Scherer's formula. It can be seen that the particle size increases with the increase in heat treatment time. The particle size calculated for different durations of heat treatment such as 3, 4, 5, and 6 are 59.1, 62.4, 63.8, and 64.3 nm respectively. Thus from the above observations we can conclude that heat treatment time is the important factor that influences the PCA of CuO/ZnO photocatalyst. It is known that calcination can increase the crystallinity of the sample, and the crystallinity will be improved with increase of the heat treatment time. The increase in photocatalytic reaction may be due to improvement in crystallinity of the sample, which is responsible for the significant separation of photogenerated electrons and holes. This result is further verified by the zeta potential measurement which is explained later in the same chapter.

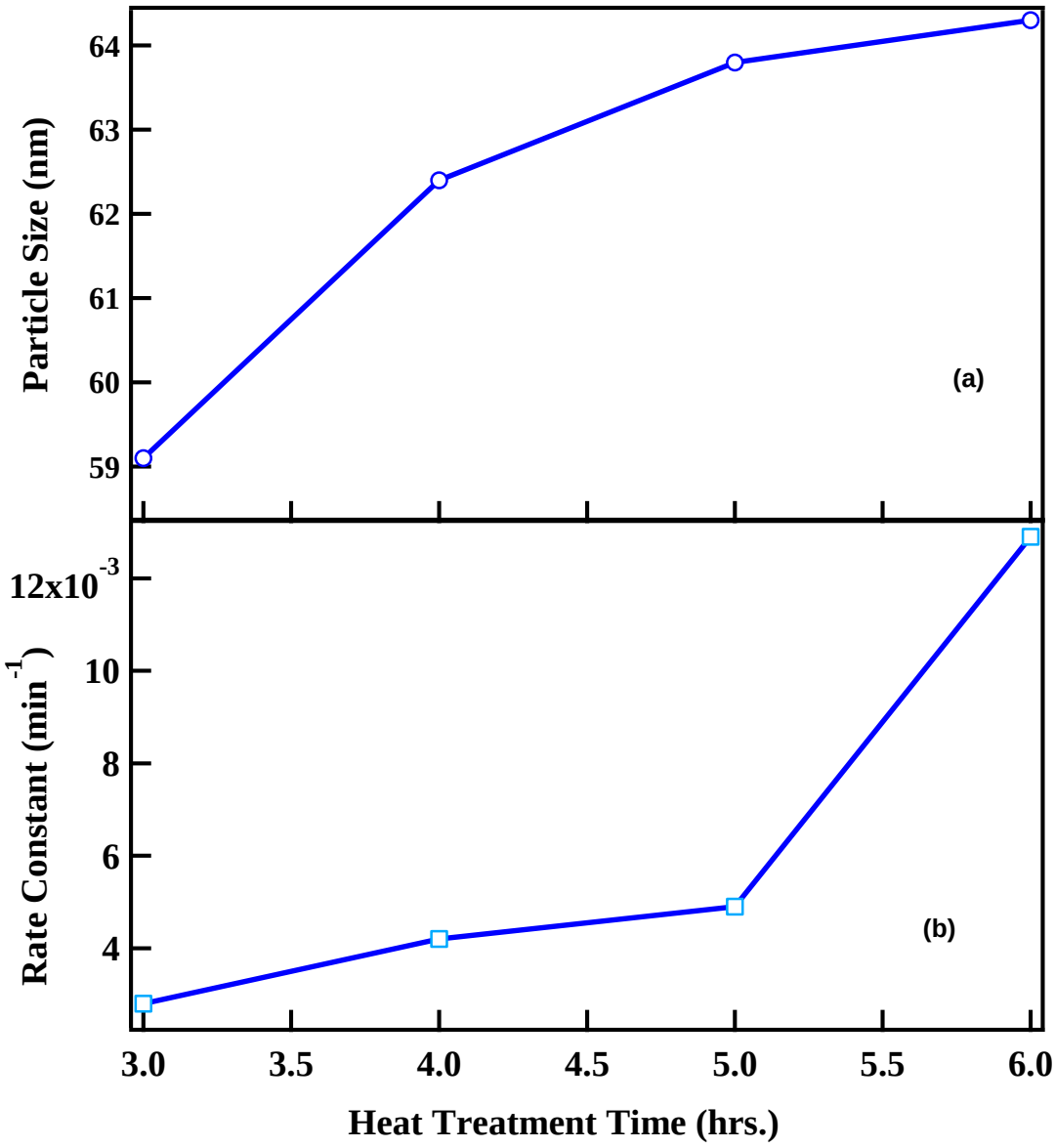


**Figure 4.14**: (a) Growth of ZnO particle size as a function of heat treatment time (700 $^{0}$C) for 12 h ball milled CuO (wt. 10%)/ZnO sample. (b) Rate constant as a function of heat treatment time for CuO (wt. 10%)/ZnO sample.

### 4.4) Zeta Potential Studies

Zeta potential (ZP) is a function of surface charge which develops when any material is placed in a liquid. In the photocatalytic process, the study of zeta potential is important because surface active electron of photocatalyst is a key factor under the illumination of light. ZP is an important parameter to predict and control dispersion stability. The magnitude of the measured zeta potential is an indication of the repulsive force that is present and can be used to predict the long-term stability of the product. If all the particles in suspension have a large negative or positive zeta potential then they will tend to repel each other and there is no tendency for the particles to come together. However, if the particles have low zeta potential values then there is no force to prevent the particles coming together and flocculating.

Figure 4.15 shows the study of zeta potential as a function of wt% of CuO in composite photocatalyst. Since pH of the solution greatly affects the measurement of zeta potential. So, the fixed pH value of the photocatalyst powder suspended in deionized water solution was maintained at ~ 7. It can be seen from Fig 4.15 that the surface of p-n junction photocatalyst p-CuO/n-ZnO is negatively charged at neutral pH. The measurement of zeta potential reveled that CuO (10 wt%)/ZnO photocatalyst provides significant negatively charged surface as compared to other composites. The high negative zeta potential observed for CuO (10 Wt.%) /ZnO signifies efficient dispersion of powder in the neutral pH solution. The well dispersed powder provides high effective surface for photooxidation of the MB. Thus, the zeta potential study further aids in explaining the effective PCA observed for CuO (10 Wt.%)/ZnO composite.

Figure 4.16 shows the study of zeta potential as a function of BM time for the CuO (10 wt%)/ZnO photocatalyst. From the Fig 4.16 it is clear that as the ball milling time increases the magnitude of the zeta potential gradually decreases. The value of the zeta potential measured for 12 hours ball milled sample was found to be -26.7 mV whereas same value measured for 72 hours ball milled sample was found to be -14.6 mV. A continuous decrease in zeta potential with increasing ball milling time evidently shows the increased agglomeration of particles which in turn reduces PCA. The result further verifies the best PCA observed for the 12 hours ball milled CuO (10 Wt.%) /ZnO sample.

Figure 4.17 illustrates the comparison study of zeta potential of CuO, ZnO, and CuO (10 Wt.%)/ZnO photocatalyst as a function of pH value. From figure it can be explained that the surface of p-n junction photocatalyst p-CuO/n-ZnO is negatively charged at neutral pH and also provides significant negatively charged surface as compared to CuO or ZnO. This study further aids in explaining the effectively high PCA observed for CuO (10 Wt.%)/ZnO composite.

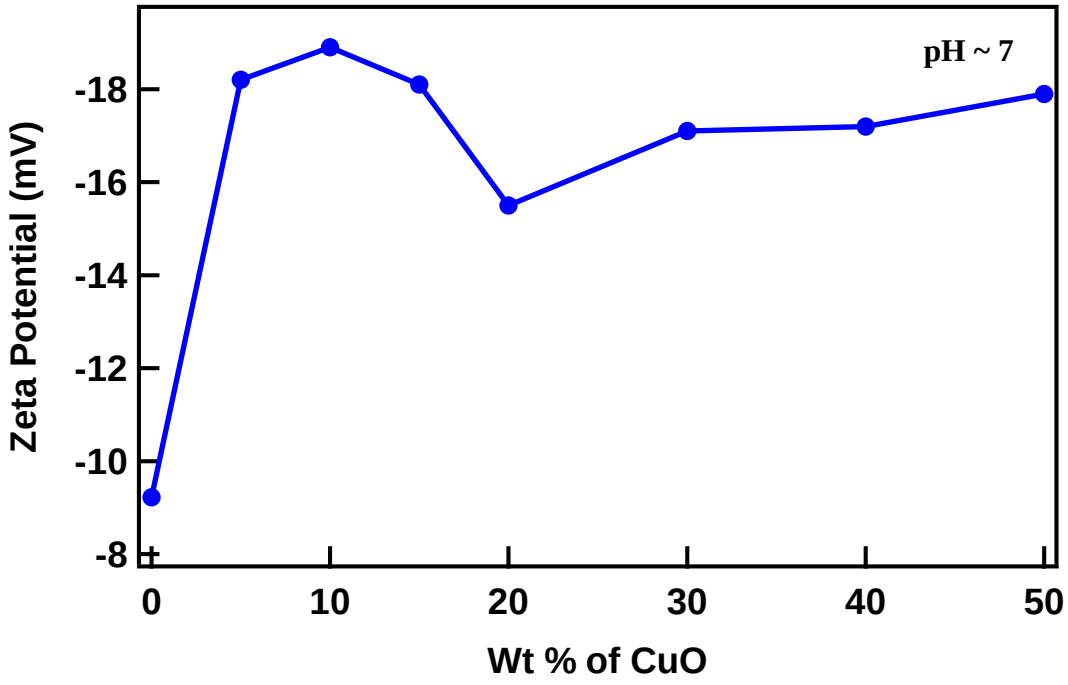


**Figure 4.15**: Zeta potential as a function of Wt.% CuO in the composite photocatalyst.

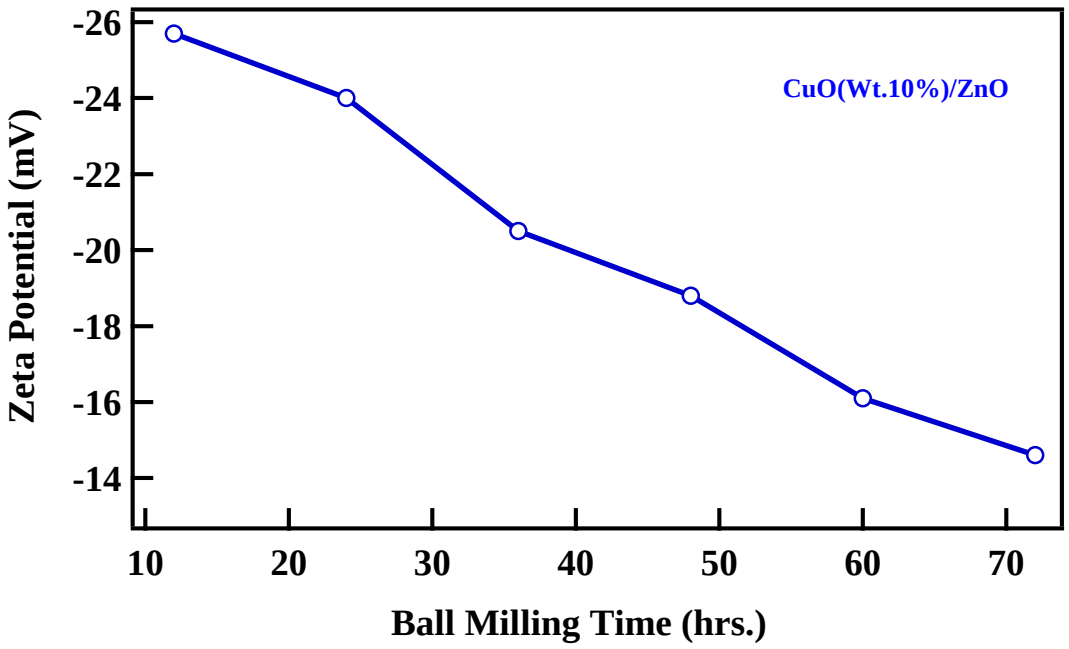


**Figure 4.16**: Zeta potential as a function ball milling time measured for CuO (10 Wt.%)/ZnO photocatalyst.

Figure 4.18 shows the zeta potential measurement of calcined CuO (10 Wt.%)/ZnO photocatalyst as a function of heat treatment time. The fixed calcined temperature was 700 $^{o}$C. From the figure it is observed that as the duration of heat treatment increases the magnitude of the zeta potential gradually increases. This result indicates that calcined sample prepared with 6 hours of heat treatment time provides significant negatively charged surface as compared to sample prepared with other shorter hours (3, 4, and 5) of heat treatment. This study further supports the higher PCA observed with 6 hours heat treatment time of sample.

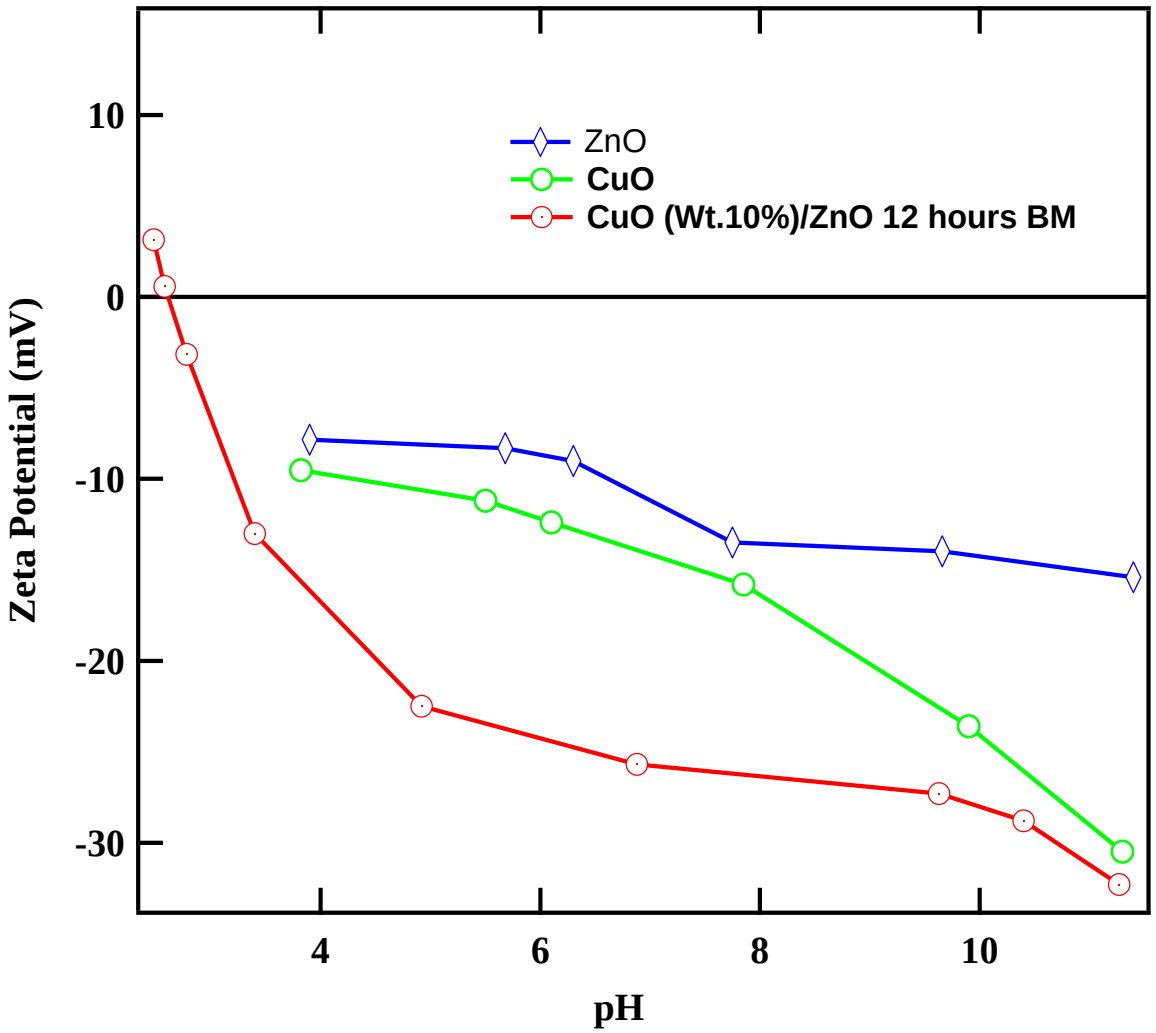


**Figure 4.17**: Comparison of zeta potential of ZnO, CuO, and 12 h BM CuO (wt. 10%)/ZnO photocatalyst as a function of pH.

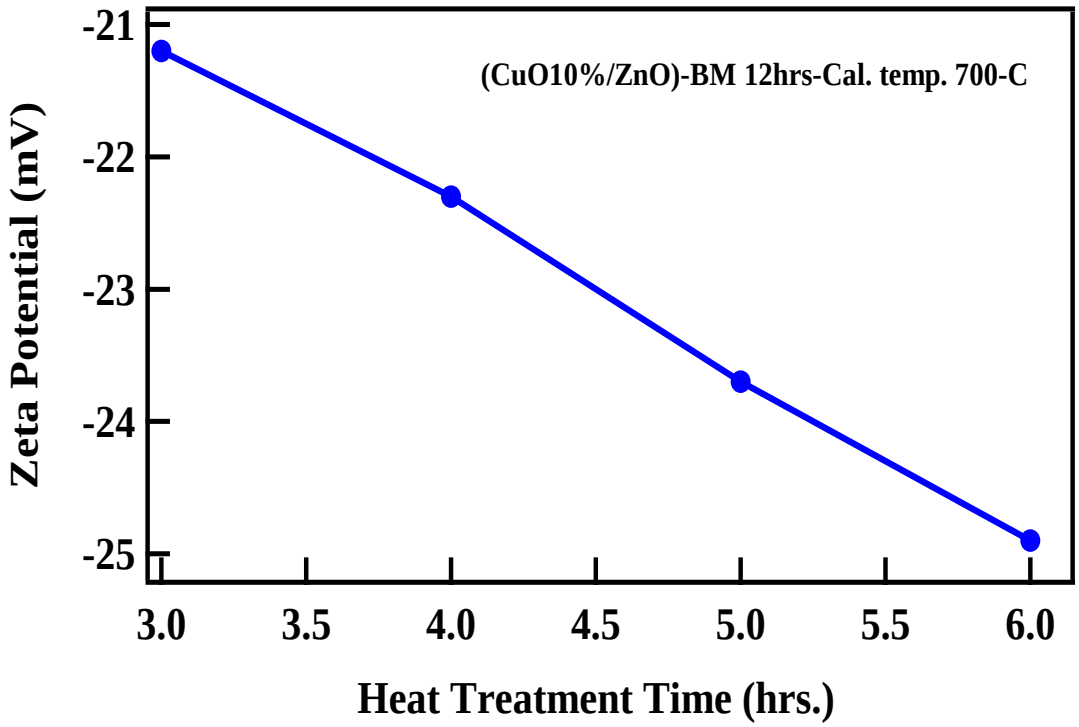


**Figure 4.18**: Zeta potential of 12 h ball milled Cuo (wt. 10%)/ZnO sample as a function of heat treatment time.

**Table 4.1**: Comparison of PCA result of our study with the similar study found in literature:

| Nanomaterials | Method | Model dye | Illumin. time | Conc. of Photocatalyst | Conc. of Model dye | Degrad. Efficiency % |
|---|---|---|---|---|---|---|
| $CuO/F\text{-}TiO_2$ [125] | wet chemical route | Rhodamine B | 20 min | 2 g/L | 0.005 g/L | 55.7 |
| $WO_3/TiO_2$ [126] | ball milling | Monocrotophos | 4 hours | 2 g/L | 0.023 g/L | 39.3 |
| $p\text{-}CuBi_2O_4/TiO_2$ [124] | solid state reaction | Methyl Orange | 20 min | 2 g/L | 0.010 g/L | 75.8 |
| $p\text{-}NiO/n\text{-}TiO_2$ [127] | sol-gel | Rhodamine B | 20 min | 2 g/L | 0.047 g/L | 62.2 |
| $p\text{-}ZnO/n\text{-}TiO_2$ [128] | ball milling | Methyl Orange | 20 min | 2 g/L | 0.030 g/L | 68.1 |
| p-Nio/n-CaO [129] | mechanically mixing | Methylene Blue | 180 min | 4 g/L | 0.010 g/L | 96.5 |
| p-NiO/n-ZnO [100] | sol-gel | Methyl Orange | 20 min | 2 g/L | 0.010 g/L | 45.7 |
| p-CuO/n-ZnO | ball milling | Methylene Blue | 15 min | 0.2 g/L | 0.005 g/L | 99.2 |

# CHAPTER 5

## CONCLUSIONS

The p-n junction oxide photocatalysts with superior photocatalytic activity were prepared by using simple ball milling technique. From XRD analysis, all the peaks of the prepared photocatalysts were clearly identified as monoclinic CuO or hexagonal wurtzite ZnO. No other impurity phase was detected during the ball milling process. The calcination of CuO (wt. 50%)/ZnO nanocomposite led to the decrease in the photocatalytic activity because of the grain growth of individual components. The PCA of CuO/ZnO nanocomposite increased remarkably with the increase in wt.% of CuO till 10 wt.% and then decreased with increasing wt.% beyond 10 wt.%.

The pH value is an important parameter that influences the PCA and the best PCA was observed at pH 7 of the solution. The concentration of the photocatalyst in the reaction solution is another important variable in the evaluation of PCA. The optimum of Cuo (wt. 10%)/ZnO photocatalyst loading for the best degradation of MB was found to be 10 mg in 50 ml of MB solution. The ball milling time also has a significant influence on the PCA of the photocatalyst. The optimum ball milling time of Cuo (wt. 10%)/ZnO photocatalyst is 12 hours. For ball milling time longer than the optimum time, the sample possesses high surface energy which leads to agglomeration, resulting in the decrease of the PCA. This result was further verified by the zeta potential measurement of all the ball milled samples. The heat treatment time also influences the PCA strongly. The photocatalytic reaction increased significantly with the increase in heat treatment time. The value of rate constant was found to increase by 360% when the heat treatment time

was increased from 3 to 6 hours. The possible reason may be due to the improvement in crystallinity of the sample with the increase in the heat treatment time.

The efficiency of the degradation of model pollutants in the presence of photocatalyst was found to be dependent on several parameters. Under optimum conditions ( pH 7, wt. of CuO (wt. 10%)/ZnO = 10 mg, wt. of MB = 1.25 mg, ball milling time = 12 h ) a 50 ml of MB solution was degraded by 100% within 15 min. The observations of these investigations clearly demonstrate the importance of choosing the optimum degradation parameters to obtain a high degradation rate, which is essential for any practical applications of photocatalytic oxidation processes. The best degradation condition depends strongly on the type of pollutants.

The observed superior activity in our study may be attributed to the well matched band edges of both p-type CuO and n-type ZnO in p-CuO/n-ZnO nanocomposites, which is suitable to promote the irreversible transfer of charge carriers, i.e. $e^-$ and $h^+$, from one semiconductor to the another semiconductor, thus suppressing the recombination of photogenerated electrons and holes. When p-type CuO and n-type ZnO integrate by ball milling, many micro p-n junction CuO/ZnO photocatalyst are engendered at the interface of the CuO and ZnO nanoparticles which may be responsible for the efficient separation of photogenerated electrons and holes. Thus this study offers a novel p-n junction oxide photocatalyst CuO (wt. 10%)/ZnO for the degradation of model dye under the illumination of UV-Vis light.

The important results obtained in our study can be summarized as follows:

1) We have demonstrated a simple ball milling route to obtain p-n junction photocatalysts with superior PCA under UV-Vis irradiation condition.
2) Our study shows that PCA of p-n junction CuO/ZnO photocatalysts can be effectively tuned by manipulating the interface of the heterostructure by adjusting the parameters affecting the PCA.
3) Study of zeta potential reveled that CuO (10 wt. %)/ZnO photocatalysts provide significant negatively charged surface as compared to other composites. This assumption is further verified by the result obtained from the PCA.
4) The observed rate-constant in CuO/ZnO composite is superior to either ZnO or CuO.
5) The optimum wt.% of CuO in the p-CuO/n-ZnO photocatalyst is 10 wt.%. When the p-CuO is higher than its optimum amount of coupling, the photocatalytic activity decreases. The result is further verified by the zeta potential measurement.
6) The photocatalytic efficacy of CuO/ZnO can be related to the presence of micro p-n junctions formed upon ball milling.
7) The pH and zeta potential study indicate that the effective particle separation is necessary to achieve high photocatalytic rate.

# CHAPTER 6

## FUTURE WORKS

The following studies can be performed in future:

1) Similar studies can be done by choosing well matched band edges of both p- and n-type oxide semiconductors from the following oxides such as ZnO, CdS, $WO_3$, $Fe_2O_3$, $TiO_2$, CuO, $ZrO_2$, ZnS, NiO, $CoFe_2O_4$, $CaFe_2O_4$, etc. These oxides have suitable band gap in UV and vis region.
2) Band-gap study of p-n junction oxide photocatalysts can be performed to further understand the optical properties of the photocatalysts and to improve their PCA. This study may help for the optimum utilization of solar energy by evaluating the band gap.
3) Surface area study of the photocatalysts can be performed to further verify the result obtained from the PCA.
4) To understand the effectiveness of the photocatalyst in actual practice, the experiment can be performed with real water containing organic pollutants in the presence of sun light.
5) The photoluminescence emission spectra can be studied to investigate the efficiency of the charge carrier trapping, immigration, and transfer since photoluminescence emission results from the recombination of free carriers.
6) Hydroxyl radical analysis can be performed by using standard photoluminescence (PL) instrument. The study of change of PL spectra of different photocatalysts can be performed for this analysis.

# CHAPTER 7

## REFERENCES:


[1] http://www.eolss.net/Sample-Chapters/C06/E6-190-16-00.pdf, April 25 (2012).

[2] N. A. Laoufi, D. Tassalit, F. Bentahar, Global NEST J. 10, (2008) 404.

[3] A. Fujishima, K. Honda, Nature, 238, (1972) 37.

[4] A. Fujishima, T. N. Rao, D. A. Tryk, J. Photochem. Photobiol.C, 1, (2000) 1.

[5] A. J. Nozik, R. Memming, J. Phys. Chem. 100 (1996) 13061.

[6] P. Fernandez, J. Blanco, S. Malato, D. L. Nieves, F. J. Water Res. 37 (2003) 3180.

[7] D.S. Bhatkhande, V.G. Pangarkar, A.A.C.M. Beenackers, , J. Chemical Tech. and Biotech. 77 (2001) 102.

[8] D.F. Ollis, E. Pelizzetti, N. Serpone, Env. Sci. and Tech. 25 (1991) 1522.

[9] http://www.observatorynano.eu/project/filesystem/files/ObservatoryNANO%20Briefing%20No.10%20Applications%20for%20Photocatalysts.pdf , May 5 (2012).

[10] http://trid.trb.org/view.aspx?id=862594 , May 8 (2012).

[11] http://www.pilkington.com/northamerica/usa/english/products/bp/bybenefit/selfcleaning/activ/home.htm , May 10 (2012).

[12] W. S. Chiu, P. S. Khiew, M. Cloke, D. Isa, T. K. Tan, S. Radiman, C. H. Chia, Chemical Eng. Jou., 158 (2010) 345.

[13] N. Daneshvar, S. Aber, M. S. Seyed Dorraji, A. R. Khataee, and M. H. Rasoulifard, World Acad. Of Sci, 29 (2007) 267.

[14] E. R Carraway, A. J. Hoffman, M. R Hoffmann, Environ. Sci. Technol. 28 (1994) 786.

[15] C. Richard, F. Bosquet, J. F. Pilichowski, J. Photochem. Photobilo, 45 (1997) 108.

[16] M. D. Driessen, T. M. Miller, V. H. Grassian, J. Mol. Catal. 131 (1998) 149.

[17] J. Villase, P. Reyes, G. J. Pecchi, Chem. Technol. Biotechnol, 72 (1998) 105.

[18] M. C. Yeber, J. Rodriguez, J. Freer, N. Durian, H. D. Mansilla, Chemosphere 41 (2000) 1193.

[19] V. Dijken, A. H. Janssen, M. H. P. Smitsmans, D. Vanmaekelbergh, K. Meijerink, Chem. Mater. 10 (1998) 3513.

[20] S. Neppolian, B. Sakthivel, M. Arabindoo, V. Palanichamy, J. Murugesan, Environ. Eng. 34 (1999) 1829.

[21] K. Gouvea, F. Wypych, S. G. Moraes, N. Duran, N. Nagata, P. Peralta, Chemosphere, 40 (2000) 433.

[22] S. Dindar, J. Icli, Photochem. Photobiol, 140 (2001) 263.

[23] R. Grorgekutty, M. K. Seery, and S. C. Pilai, J. Phys. Chem. C, 112 (2008) 13563.

[24] N. J. Renault, P. Pichat, A. Foissy, R. Mercier, J. Phys. Chem. 90 (1986) 2733.

[25] A. L. Linsebigler, G. Lu, and J. T. Yates, Chem. Rev. 95 (1995) 755.

[26] R. S. Sonawane, M. K. Dongare, J. Mol. Catal. A, 243 (2006) 68.

[27] J. M. Jung, M. Wang, E. J. Kim, S. H. Hahn, Vacuum 82 (2008) 827.

[28] E. C. Butler, A. P. Davis, J. Photochem. Photobiol. 70 (1993) 273.

[29] M. Fujihira, Y. Satoh, T. Osa, Bull. Chem. Soc. Jpn. 55 (1982) 666.

[30] J. M. Herrmann, J. Disdier, P. Pichat, Chem. Phys. Lett. 108 (1984) 618.

[31] H. Gerischer, F. Willig, Top. Curr. Chem. 61 (1976) 31.

[32] P. V. Kamat, M. A. Fox, Chem. Phys. Lett. 102 (1983) 379.

[33] C. Shifu, C. Lei, G. Shen, C. Gengyu, Mat. Chem. and Phy. 98 (2006) 116.

[34] C. Shifu, C. Lei, G. Shen, C. Gengyu, Power Tech. 160 (2005) 198.

[35] B. Patrick, P. V. Kamat, J. Phys. Chem. 96 (1992) 1423.

[36] N. Vlachopoulos, P. Liska, J. Augustynski, M. J. Gratzel, J. Am. Chem. Soc. 110 (1988) 1216.

[37] A. A. Kdash, A. Idris, K. Saed, C. T. Guan, Global Nest, 6 (2004) 223.

[38] Anna Goi, Thesis, Tallinn Univ. of Tech. 1 (2005) 45.

[39] F. He, X. Shen, L. C. Lei, J. Eniv. Sci. 15 (2003) 351.

[40] O. Legrini, E. Oliveros, A. M. Braun, Chem. Rev. 93 (1993) 671.

[41] M. R. Hoffmann, S. T. Martin, W. Y. Choi, and D. W. Bahnemann, Chem. Rev. 95 (1995) 69.

[42] M. A. Fox, M. T. Dulay, Che. Rev. 93 (1993) 341.

[43] L. Cesar, A. Kay, J. A. G. Martinez, M. J. Gratzel, J. of Am. Chem. Soc. 128 (2006) 4582.

[44] S. F. Chen, G. Y. Cao, Chem. Phys. Lett. 413 (2005) 404.

[45] A. Eslami, S. Nasseri, B. Yadollahi, A. Mesdaghinia, F. Vaezi, R. Nabizadeh, S. Nazmara, J. Chem. Technol. Biotechnol. 83 (2008) 1447.

[46] C. Hariharan, Appl. Catal. 304 (2006) 55.

[47] C. Lizama, J. Freer, J. Baeza, H. D. Mansilla, Catal. Today, 76 (2002) 1.

[48] N. Daneshvar, D. Salari, A. R. Khataee, J. Photochem. Photobiol. A, 157 (2003) 111.

[49] S. Sakthivel, B. Neppolian, M. V. Shankar, B. Arobindoo, M. Palanichamy, V. Murugesan, Solar Energ. Mater. Solar Cells, 77 (2003) 65.

[50] N. Daneshvar, D. Salari, A. R. Khataee, J. Photochem. Photobiol. A, 162 (2004) 317.

[51] M. H. Habibi, H. Vosooghian, J. Photochem. Photobiol. A, 174 (2005) 45.

[52] W. Y. Su, Y. F. Zhang, Z. H. Li, L. Wu, X. X. Wang, and J. Q. Li, Langmuir 24 (2008) 3422.

[53] C. C. Chen, H. J. Fan, and J. L. Jan, J. Phys. Chem. C, 112 (2008) 11962.

[54] X. Wang, W. Lian, X. Fu, J. M. Basset, J. Catal. 238 (2006) 13.

[55] G. Marcı, V. Augugliaro, M. J. L. Munoz, J. Phys. Chem. B 105 (2001) 1033.

[56] Y. Zheng, C. Chen, Y. Zhan, X. Lin, Q. Zheng, and J. Zhu, J. Phys. Chem. C 112 (2008) 10773.

[57] X. Q. Qiu, L. P. Li, X. Z. Fu, and G. S. Li, J. Nanosci. Nanotech. 8 (2008) 1301.

[58] H. Tang, J. C. Chang, Y. Shan, and S. T. Lee, J. Phys Chem B 112 (2008) 4016.

[59] Z. Wen, G. Wang, W. Lu, Q. Wang and J. Li, Cryst. Growth Design. 7 (2007) 1722.

[60] Z. Zhang, Y. Yuan, Y. Fang, L. Liang, H. Ding, and L. Jin, 73 (2007) 532.

[61] H. P. Klug and L. E. Alexander, X-ray diffraction procedures for polycrystalline and amorphous materials. Wiley, New York, Vol. 1 (1997).

[62] R. Asahi, T. Morikawa, T. Ohwaki, K. Aoki, Y. Taga, Science, 293 (2001) 269.

[63] S. Liu, C. Li, J. Yu, Q. Xiang, Cryst. Eng. Comm. 13 (2011) 2533.

[64] K. Cham, J. D. Seok, G. L. Se, J. L. Sung,Y. K. Ho, Appl. Catal. Gen. 330 (2007) 127.

[65] X. Chen, C. Budra, J. Phys. Chem. B, 108 (2004) 15446.

[66] M. O. Henry, J. P. Mosnier, Superlattices Microstruct. 42 (2007) 74.

[67] M. Shinya, I. Tadaaki, A. Kimio, Q. W. Zhang, S. Fumio, T. K. Shozo, Chem. Phys. Lett. 436 (2007) 373.

[68] X. Wang, P. Hu, Y. Fangli, L. Yu, J. Phys. Chem. C, 111 (2007) 6706.

[69] K. C. Hsiao, S. C. Liao, Y. J. Chen, Mater. Sci. Eng. A, 447 (2007) 71.

[70] R. H. Wang, J. H. Xin, Y. Yang, H. F. Liu, L. M. Xu, J. H. Hu, Appl. Surf. Sci. 227 (2004) 312.

[71] K. G. Kanade, B. B. Kale, J. O. Baeg, S. M. Lee, C. W. Lee, S. J. Moon, H. Chang, Mater. Chem. Phys. 102 (2007) 98.

[72] S. Sakthivel, S. U. Geissen, D. M. Bahnemann, V. Murugesan, A. Vogelpohl, J. Photochem. Photobiol. Chem. 148 (2002) 283.

[73] Y. H. Zheng, L. R. Zheng, Y. Y. Zhan, X. Y. Lin, Q. Zheng, K. M. Wei, 46 (2007) 6980.

[74] J. Han, L. Y. Shi, R. M. Cheng, Y. W. Chen, P. F. Dong, Q. W. Shao, Chinese J. Inorg. Chem. 24 (2008) 950.

[75] P. Kundu, P.A. Deshpande, G. Madras, N. Ravishankar, J. Mater. Chem. 21 (2011) 4209.

[76] Q. Sun, Y. Xu, J. Phys. Chem. C, 113 (2010) 12387.

[77] Y. Park, S. H. Lee, S. O. Kang, W. Choi, Chem. Commun., 46 (2010) 2477.

[78] K. S. Yao, D. Y. Wang, C. Y. Chang, W. Y. Ho, L. Y. Yang, J. Nanosci. Nanotechnol. 8 (2008) 2699.

[79] K. W. Kwon, B. H. Lee, M. Shim, Chem. Mater. 18 (2006) 6357.

[80] W. Shi, H. Zeng, Y. Sahoo, T. Y. Ohulchanskyy, Y. Ding, Z. L. Wang, M. Swihart, P. N. Prasad, Nano. Lett. 6 (2006) 875.

[81] N. M. Huang, C. S. Kan, P. S. Khiew, S. Radiman, J. Mater. Sci. 39 (2004) 2411.

[82] J. Zhu, D. Yang, J. Geng, D. Chen, Z. Jiang, J. Nanopart. Res. 10 (2008) 729.

[83] G. S. Li, D. Q. Zhang, J. C. Yu, Enivron. Sci. Technol. 43 (2009) 7079.

[84] L. C. Sha, T. Y. Ping, K. Bonan, W. Binsong, Z. Feng, M. Qiang, X. Ji, W. Dazhi, L. Ji, Sci. China, 50 (2007) 279.

[85] L. Wu, J. C. Yu, X. Fu, J. Mol. Catal. A, 244 (2006) 25.

[86] C. Shifu, Z. Wei, L. Wei, Z. Sujuan, J. Sol-Gel. Sci. Technol. 50 (2004) 387.

[87] A. Hameed, T. Montini, V. Gombaca, P. Fornasiero, Photochem. Photobio. Sci. 8 (2009) 677.

[88] Z. Zhang, C. Shao, X. Li, C. Wang, M. Zhang, Y. Liu, Applied Materials and Interfaces, 2 (2010) 2915.

[89] B. Li, Y. Wang, Superlattices and Microstruc. 47 (2010) 615.

[90] H. Ohta, M. Hirano, K. Nakahara, H. Maruta, T. Tanabe, M. Kamiya, H. Hosono, Appl. Phys. Lett. 83 (2003) 1029.

[91] J. Wang, C. Lee, Y. Chen, C. Chen, C. Lin, Appl. Phys. Lett. 95 (2009) 131117.

[92] C. Shifu, C. Lei, G. Shen, C. Gengyu, Materials Chemisry and Physics, 98 (2006) 116.

[93] S. F. Chen, S. J. Zhang, W. Liu, W. Zhao, J. Hazard. Mater. 155 (2008) 320.

[94] T. Aarthi, G. Madras, Ind. Eng. Chem. Res. 46 (2007) 7.

[95] K. Rajeshwar, M. E. Osugi, W. Chanmanee, C. R. Chenthamarakshan, M. V. B. Zanoni, P. Kajitvichyanukul, R. Krishnan, J. Photochem. Photobiol. C, 9 (2008) 171.

[96] C. N. J. Wagner and E. N. Aqua, Adv. X-ray Anal. 7 (1964) 46.

[97] http://www.ucmo.edu/chemphys/about/documents/cary_300_bio_uv.pdf , May 25 (2012).

[98] V. L. Colvin, M. C. Schlamp, A. P. Alicisatos, Nature, 370 (1994) 354.

[99] J. H. Park, J. Y. Kim, B. D. Chin, Y. C. Kim, O. O. Park, Nanotechnology, 15 (2004) 1217.

[100] C. Shifu, Z. Wei, L. Wei, Z. Sujuan, J. Sol-Gel Sci. Technol. 50 (2009) 387.

[101] L. Wei, C. Shifu, Z. Sujuan, Z. Wei, Z. Huaye, Y. Xiaoling, J. Nanopart. Res. 12 (2010) 1363.

[102] N.T Nolan, Doctoral Thesis, Dublin Institute of Technology, 1 (2010) 48.

[103] Z. Zhenyi, C. Shao, L. Xinghau, W. Changhua, Z. Mingyi, and Y. Liu, Amer. Chem. Soc. 2 (2010) 388.

[104] W. Liu, S. Chen, Z. Sujuan, Z Wei, Z. Huaye, Y. Xiaoling J Nanopart Res, 12 (2010) 1355.

[105] S. Chen, W. Zhao, W. Liu, and S. Zhang, Appl. Surf. Sci. 255 (2008) 2478.

[106] L. M. Chen, X. M. Sun, Y. N. Liu, Y. D. Li, Appl. Catal. A: Gen. 265 (2004) 123.

[107] C. Minero, G. Mariella, E. Pelizzetti, Langmuir, 16 (2000) 2632.

[108] M. Qumar, M. Muneer, Desallination, 249 (2009) 535.

[109] N. Daneshvar, S. Aber, M. S. Seyed Dorraji, A. R. Khataee, M. H. Rasoulifard, World Academy of Science, 29 (2007) 267.

[110] J. S. Reed, Introduction to the principles of ceramic processing, John Wiley and Sons, New York, 1 (1986).

[111] J. Biscan, M. Kosec, Kovine, Zlitinem technologije, 29 (1996) 170.

[112] A. A. Khodja, T. Sehili, J. F. Pilichowski, P. Boule, J. Photochem. Photobiol. A, 141 (2001) 231.

[113] A. Akyol, M. Bayramoglu, J. Hazard. Mater. B, 124 (2005) 241.

[114] S. Kaneco, H. Katsumata, T. Suzuki, K. Funasaka, K. Ohta, Bull. Catal. Soc. Ind. 6 (2007) 22 .

[115] U. Stafford, K. A. Gray, P. V. Kamat, J. Catal. 167 (1997) 25.

[116] M. Munner, H. K. Singh, D. W. Bahnemann, Chemosphere, 49 (2002) 193.

[117] M. Qumar, M. Saquib, M. Munner, Dyes and Pigments, 65 (2005) 1.

[118] N. Deneshwar, M. H. Rasoulifard, A. R. Khataee, F. Hosseinzadeh, J. Hazard. Mater. 143 (2007) 95.

[119] W. Liu, S. Chen, Z. Sujuan, Z Wei, Z. Huaye, Y. Xiaoling J Nanopart Res, 12 (2010) 1355.

[120] S. Chen, W. Zhao, W. Liu, and S. Zhang, Appl. Surf. Sci. 255 (2008) 2478.

[121] L. M. Chen, X. M. Sun, Y. N. Liu, Y. D. Li, Appl. Catal. A: Gen. 265 (2004) 123.

[122] J. Wang, S. Yin, M. Komatsu, Q. Zhang, F. Saito, and T. Sato, J. Photochem. Photobio. A, 164 (2003) 155.

[123] M. Gratzel, J. Photochem. Photobio. A, 165 (2004) 149.

[124] L. Wei, C. Shifu, Z. Sujuan, Z. Wei, Z. Huaye, Y. Xiaoling, J. Nanopart. Res, 12 (2010) 1355.

[125] Z. Jinfeng, Y. Yunguang, L. Wei, International J. of Photoenergy, 2012 (2011) 1.

[126] C. Shifu, C. Lei,G. Shen, C. Gengyu, Powder Technology, 160 (2005) 198.

[127] C. Shifu, Z. Sujuan, L. Wei, Z. Wei, J. of Hazardous Materials, 155 (2008) 320.

[128] C. Shifu, Z. Wei, L. Wei, Z. Sujuan, Applied Surface Science, 255 (2008) 2478.

[129] L. Song, S. Zhang, J. of Hazardous Materials, 174 (2010) 563.